Thesis/
Reports
Catchpole,
W.R.

Second generation...

FINAL REPORT FOR RESEARCH AGREEMENT
#INT-94962-RJVA
"Fire Spread Model Development
AUSTRALIA: UNIVERSITY OF NEW SOUTH WALES
FS Contact: Dr. Bret W. Butler
CoOp Contact: Dr. Wendy Catchpole

US FOREST SERVICE–ADFA

JOINT RESEARCH VENTURE

RMRS-94962-RJVA

FINAL REPORT

January 2000

W.R. & E.A. Catchpole

"This research was supported in part by funds provided by the Rocky Mountain Research Station, Forest Service, U.S. Department of Agriculture."

The Second Generation U.S. Firespread Model — Final Report 1999

W.R. and E.A. Catchpole

School of Mathematics and Statistics, University College UNSW,
Australian Defence Force Academy, Canberra, ACT 2600, Australia

January 7, 2000

Part 1: The model

1. Volume element

We develop a model for the steady spread of fire through a homogeneous fuel bed. The fuel bed is modelled as an arrangement of homogeneous particles all with the same moisture content m at ambient temperature. The role of the air between the fuel particles is to supply oxygen; the thermal capacity of this air is neglected.

Most models concentrate on an energy balance for a small volume element containing fuel particles and air, as shown in Figure 1. Some models position this volume element next to the upper surface of the fuel bed (a), some place it within the fuel bed (b), and others assume it to have small dimensions in the horizontal directions but extend from the top to the bottom of the fuel (c). Here we consider only a surface volume element (a). The reason for this is discussed below. To each element is associated a temperature depending on its position and the time since initial ignition of the fuel bed.

The model is based on the following description of flame propagation. Combustion releases heat energy from the region of burning fuel. Some of this heat is absorbed by the unburned fuel causing its temperature to rise. When the fuel temperature of a volume element reaches a critical value $T_{\rm ig}$ (the ignition temperature) the particles in the element emit ignitable gases. These are ignited by pilot ignition and the particle moves into the combustion zone, and is consumed by an exothermic combustion process. The line on the upper surface of the fuel bed separating burning fuel from unburned fuel gives the position of the fire front. This fire front propagates at a steady speed.

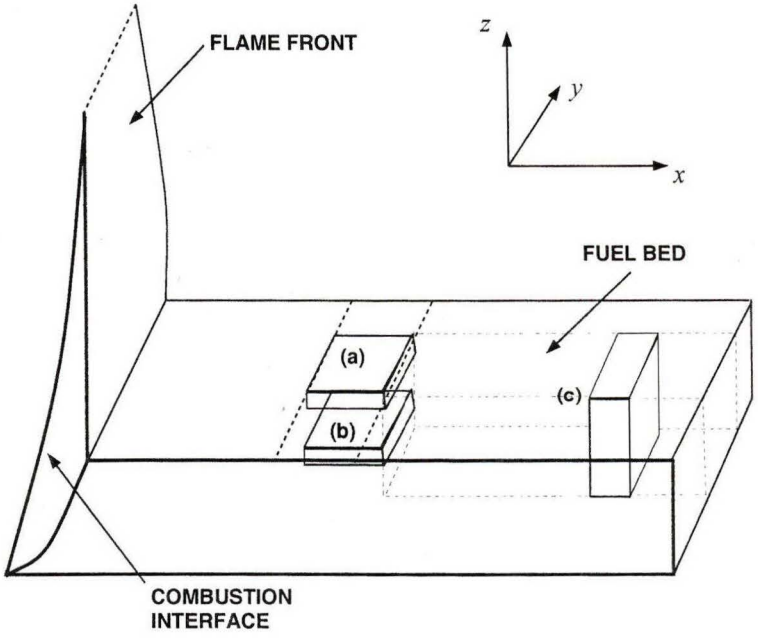

Figure 1. (a) Volume element on the surface; (b) volume element within the fuel bed; (c) total-depth element

2. Ignition temperature

During the heating of such fuel particles, each particle is assumed to be at uniform temperature throughout its volume. For non-fine fuels this assumption is unrealistic, and modifications will be discussed later.

Far away from the fire the particles are at ambient temperature but, as the flame front approaches, the particles increase in temperature until the boiling point of water is reached. At this stage we might adopt the simple assumption that further input of heat energy firstly drives off all the water at this temperature and then raises temperature of the dry fuel element to ignition. The heat required to raise the fuel-element temperature in the models is illustrated schematically in Figure 2. Thus the relationship between heat and temperature is step-wise linear.

More precisely, if a net amount of heat dQ per unit mass of fuel bed is transferred from the combustion zone or flame to the fuel bed element, then the corresponding rise in

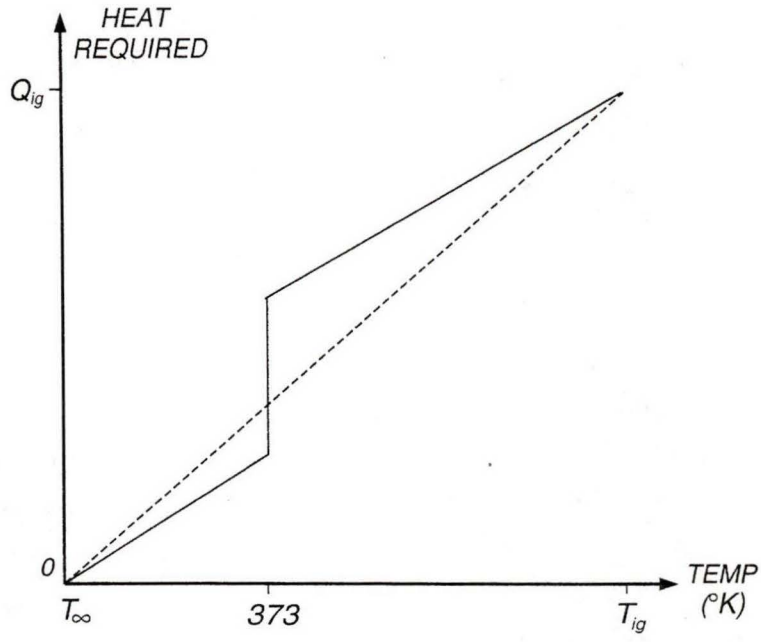

Figure 2. Heat required to raise unit mass of fuel from ambient to ignition temperature, versus fuel temperature attained. The vertical step is due to the latent heat of water.

temperature dT is given by (see e.g.de Mestre et al., 1989)

$$dQ = \begin{cases} (c_p + mc_w)dT, & T_\infty < T < 373 \\ -\mathcal{L}dm, & T = 373 \\ c_p dT, & 373 < T < T_{\text{ig}} \end{cases} \tag{1}$$

where

c_p = specific heat of dry fuel

c_w = specific heat of water

$\mathcal{L}$ = latent heat of water

m = moisture content of fuel
= mass of water per unit mass of fuel

A simpler model for the rise of temperature with heat input is just to assume a linear relationship:

$$dQ = c^* dT, \quad T_\infty < T < T_{\text{ig}}, \tag{2}$$

as shown by the dashed line in Figure 2. Here c^* denotes an "average specific heat", which accounts also for the latent heat of water. Its value is found by integrating (1) and (2) from ambient temperature T_∞ to ignition temperature $T_{\rm ig}$:

$$Q_{\rm ig} = (c_p + mc_w)(373 - T_\infty) + \mathcal{L}m + c_p(T_{\rm ig} - 373) \tag{3}$$

$$= Q_f + m\{c_w(373 - T_\infty) + \mathcal{L}\}$$

$$= c^*(T_{\rm ig} - T_\infty) \tag{4}$$

where $Q_f = c_p(T_{\rm ig} - T_\infty)$ is the quantity of heat required to raise unit mass of dry fuel to ignition temperature, and $Q_{\rm ig}$ is the quantity of heat required to raise unit dry mass of moist fuel to ignition temperature, sometimes called the "heat of ignition" of the fuel. Equation (3) was given by Dunlap (1912). Experiments indicate that for typical fuels equation (2) is a better approximation of particle temperature rise than (1) — see de Mestre et al. (1989).

A crucial but frequently unstated assumption in almost all physical models of fire spread is that there is a well-defined ignition temperature, at which a particle bursts into flame regardless of preceding conditions. In particular, ignition takes place at this temperature regardless of how quickly or slowly the particle has been heated. Since water vapour is the first pyrolisate, a particle heated slowly will have lost almost all moisture before ignitable gases are given off; a rapidly heated particle on the other hand will still be losing water vapour from its deeper layers while the surface is giving off ignitable gas. These gases will therefore be diluted with water vapour, and may require a higher temperature to ignite them.

It is thus possible that ignition temperature increases as the rate of spread increases. The magnitude of this effect in unknown; to our knowledge no experiments have explored this. The most relevant results are those of Frandsen (1973).

3. Heat transfer mechanisms

(i) Radiative heating

All models of heat transfer from the flame to the fuel element include radiative heating. Some models also include convective heating — both short-range heating by hot gases emerging from the flame front (flame contact, or turbulent diffusion), and, for wind-driven fires, the longer-range heating caused by hot air from the flaming region being advected over the unburned fuel.

As with most previous models, we treat radiation from the flame as emanating from an opaque surface coincident with the average position of the front of the flame. This surface is taken to be a plane of finite length and finite or infinite width, inclined at an angle ϕ_f (say) to the vertical. In a wind blown fire ϕ_f is positive.

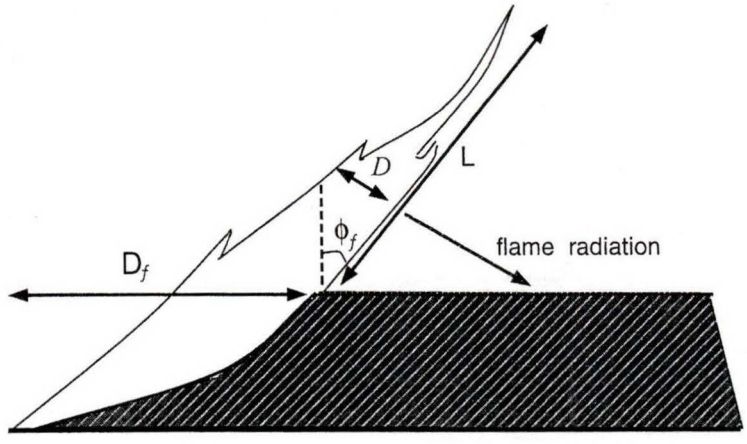

Figure 3. Radiation from a diffuse flame, showing two possible measures of flame depth.

The flame surface is taken to radiate as a grey body, with a (nominal) surface temperature T_f and emissivity ϵ_f. These may depend on height above the fuel surface. The hemispherical rate of radiation from a given point on the flame surface will then be given by

$$E_f = \epsilon_f \sigma_B T_f^4 \tag{5}$$

per unit area of flame surface, where σ_B is the Stefan-Boltzmann constant.

A more accurate model might treat the flame radiation as gas phase radiation. The standard model for a uniform gas gives

$$\epsilon_f = 1 - e^{-kD}, \tag{6}$$

where D is the width of the flame in the direction of a particular beam, as shown in Figure 3. The opacity constant k depends on the amount of soot and other radiating particles in the flame.

Note that this approaches zero for a very small D and approaches 1 (the value for a perfect black body radiator) for very thick flames. Thus ϵ_f varies not only with distance above the fuel bed but also with the direction of the beam of radiation. Such a model would be very difficult to implement. As a compromise, we could model the radiation from the flame as coming from a solid sheet, but acknowledge the diffuse nature of the flame by assuming that the flame sheet has an emissivity ϵ_f given by (6), where $D = D_f$, the flame depth in a horizontal direction at the base of the flame (see Figure 3).

We model the radiation from the combustion zone in a similar way to that from the flame, by assuming that the combustion interface is a plane, inclined at an angle ϕ_i to

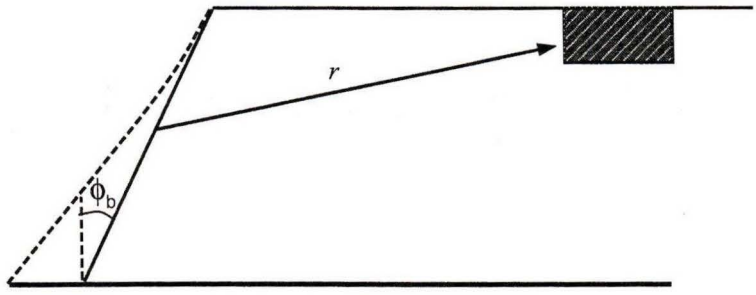

Figure 4. Radiation from the combustion interface to a surface fuel element.

the vertical, and that the radiation can be approximated by that from a solid sheet on this plane, at temperature T_b and of emissivity ϵ_b. Although combustion interfaces are known to be curved in general (see for example Albini, 1985, 1986), the error caused by our assumption will be small in most cases, since we are considering only the heat received by a surface fuel element (see Figure 4).

There are two commonly used approaches to modelling the absorption of radiation from the flame by the fuel, which we term "surface heating" and "volume heating". In the surface-heating mechanism the radiation is transmitted (undiminished) from the flame front to the surface of the unburned fuel bed. The fuel surface heats up and acts as a source which then heats the remainder of the fuel bed.

The volume-heating mechanism is more realistic but mathematically more difficult. It postulates a semi-transparent fuel bed through which the rays penetrate until they meet a fuel particle, which absorbs the radiation and rises in temperature. Thus the radiation gradually diminishes as it passes through the fuel bed. This model is greatly simplified if the fuel particles are assumed to act as black-body absorbers, so that there is no reflection or scattering of radiation.

The mathematical law appropriate for the absorption of a beam of radiation through such a semi-transparent medium is that of exponential decay,

$$i = i_0 e^{-\alpha r} \tag{7}$$

where i is the intensity of a beam of radiation, r is the distance that the beam has travelled through the fuel bed, and α is a decay constant (α^{-1} is the mean free path length for radiation through the fuel). For a collection of randomly oriented, black, convex particles, it can be shown (see e.g. Hottel et al., 1965) that $\alpha = s\beta/4$, where s is the surface-area to volume ratio of the particles and β is the packing ratio, so that $s\beta$ is the surface area of fuel per unit volume of fuel bed.

(ii) Convective heating

The rate of convective heat input per unit volume of fuel bed is

$$q_c = \hbar s \beta (T_a - T), \tag{8}$$

where $\hbar$ is the convective heat transfer coefficient, T is the temperature of the particles in the unit volume, and T_a is the temperature of the surrounding gas. This gas may range from a mixture of air and pyrolised gases at flame temperature, moving at fairly high velocity and turbulent, to still air at ambient temperature (in which case q_c becomes a cooling term).

The convective heat transfer coefficient $\hbar$ depends mainly on particle size and on the gas velocity. For forced convection (i.e. with an ambient air flow past the particle), it can be calculated from empirical formulæ relating the Nusselt and Reynolds numbers. The Nusselt number

$$N_u = \frac{\hbar \ell}{k} \tag{9}$$

is a dimensionless measure of the gas temperature gradient at the fuel surface. Here k is the thermal conductivity of the gas, and ℓ is a characteristic fuel particle dimension. The Reynolds number

$$R_e = \frac{U_0 \ell}{\nu} \tag{10}$$

is the ratio of inertial to viscous force. Here U_0 is the gas flow speed past the particles and ν is the kinematic viscosity of the gas.

For example, for a cylindrical particle in a crossflow, using $\ell = d$, the particle diameter, Incropera and De Witt (1990, eqn. 7.56) give an empirical relation which reduces, for air at atmospheric pressure in the range 300–1000 K, to

$$N_u \approx 0.66 R_e^{0.4}, \tag{11}$$

valid for $1 < R_e < 40$. This gives

$$\hbar \approx 0.66 k \nu^{-0.4} d^{-0.6} U_0^{0.4} \approx 0.29 k \nu^{-0.4} s^{0.6} U_0^{0.4}, \tag{12}$$

where we have used $s \approx 4/d$ for a long thin cylinder. For a particle of diameter 1 mm, typical of pine needles, the range $1 < R_e < 40$ corresponds to a gas velocity of roughly 0.05–2 m/sec, depending on the gas temperature. The general form of the relationship is

$$N_u \approx c R_e^m, \tag{13}$$

where the values of c and m depend on the range of the Reynolds number, and the shape of the cross-section of the particle (Incropera and De Witt, 1990, eqn. 7.56). More complicated empirical relations are available which cover the entire range of Reynolds numbers for which data are available (see e.g. Incropera and De Witt, 1990, eqn. 7.57).

(iii) Heat losses

Loss due to re-radiation from the element varies as $T^4 - T_\infty^4$, the difference between the fourth powers of the absolute temperature of the element and that of the environment. Heat loss due to convective cooling by the surrounding air (assumed to be at ambient temperature) is proportional to the difference $T - T_\infty$. A calculation by Albini (1986) showed that the natural convective cooling of foliage is of comparable magnitude to the radiative cooling, throughout the range from ambient to ignition temperature.

4. Energy balance equations

The model is based on the energy balance of a typical fuel surface volume element. The net effect of heat input and heat loss in a small interval of time is equated to the corresponding increase in internal energy of the fuel element as given by (1).

This energy balance leads to a differential equation for the average temperature of the volume element, which contains the rate of spread as a parameter. When the rate of spread is assumed constant, the differential equation can be integrated as the flame front moves from the far distance, when the temperature of the volume element is ambient, towards the volume element. When the flame reaches the volume element, the temperature reaches ignition temperature and the volume element bursts into flame. This is often referred to as an integrated or global energy balance.

A simple approach to the derivation of the differential equation is as follows. Consider a volume element at location (x, y, z) in the fuel bed, where the coordinate system is as shown in Figure 1 — thus x is measured in the same direction as the fire propagation, y is horizontal, parallel to the flame front, and z is vertical. Let the temperature, at time t, of the fuel particles in the volume element be $T(x, y, z, t)$, and the corresponding heat content be $Q(x, y, z, t)$ per unit dry mass of fuel. The heat content *per unit volume* of fuel bed is then $\rho_b Q$, where ρ_b is the bulk density of the fuel bed, that is the dry mass of fuel per unit volume of fuel bed. In the 2-dimensional situation, where the fire front is straight and infinitely wide, the temperature cannot depend on the lateral position of the fuel particle and so we have $T(x, z, t)$ only. The rate of temperature rise $\partial T/\partial t$ of the fuel element is

then related to the net rate of heat absorption per unit volume of fuel bed, $\partial Q/\partial t$, by

$$\frac{\partial Q}{\partial t} = c^* \frac{\partial T}{\partial t}, \tag{14}$$

as in (2).

We consider only the quasi-steady case, when the fire has reached a steady rate of spread R. In this case the distance X of the volume element from the flame front is decreasing linearly with time

$$X = X_0 - Rt,$$

and it follows that

$$\frac{\partial T}{\partial t} = -R \frac{\partial T}{\partial X}.$$

The coordinates (X, z) define a moving coordinate system, in which the flame front is fixed and the fuel element approaches the flame front at speed R. In this new coordinate system the rate of heat absorption is given by

$$\frac{\partial Q}{\partial t} = -R \frac{\partial Q}{\partial X} = -Rc^* \frac{\partial T}{\partial X}. \tag{15}$$

The modelling effort then focusses on modelling the heat transfer processes from the flame and combustion zone to the fuel element (and heat losses from the fuel element), in order to find $\dfrac{\partial Q}{\partial t}$. Once this is done, the governing differential equation takes the form

$$-R\rho_b c^* \frac{\partial T}{\partial X} = q(X, z), \tag{16}$$

where $q(X, z)$ is the net rate of heat input per unit volume of fuel bed at the point (X, z). This net heat inflow is broken down according the the heat transfer mechanism,

$$q = q_r + q_c - q_\ell, \tag{17}$$

where $q_r = q_f + q_i$ is the total radiant heat input (energy per unit time per unit volume) into the volume element, q_f and q_i being the contributions from the flame and combustion zone, respectively; q_c is the convective heat transfer, and q_ℓ is the radiative heat loss from the fuel element. Note that q_c may be positive (in a wind-driven fire) from hot air which has passed through the combustion to the fuel (advective heating) or due to short range (diffusive) heating caused by turbulence in the flame, or it may be negative to account for heat loss from the warm fuel to the surrounding cooler air; or it may account for all of

these, for example switching from negative (cooling) far away from the flame to positive (heating) close to the flame.

Integrating (16) over the whole of the unignited portion of the fuel bed gives

$$RwQ_{\rm ig} = \int\int q(X,z)\,dXdz, \tag{18}$$

where $w = \rho_b\delta$ is the total fuel loading per unit area of the fuel bed, δ being the depth of the fuel bed. This is the integrated energy balance equation. It states simply that the rate at which fuel is being heated to ignition temperature, and consumed in the combustion zone, is equal to the total net rate of heat transfer from the combustion zone and flames into the unignited portion of the fuel bed.

Equation (18) can also be written

$$I_P = \frac{1}{\delta}\int\int q(X,z)\,dXdz, \tag{19}$$

where $I_P = R\rho_b Q_{\rm ig}$ is the *propagating flux*, which can be thought of as the rate of transfer of sensible heat through a unit surface area perpendicular to the direction of flame travel.

For non-fine fuels the left-hand side of (18) overestimates the amount of heat absorbed by the fuel during the preheating process. Many authors replace w in (18) by w_a, the actual amount of fuel consumed in the fire. This is certainly an improvement, but is still an overestimate. Better is to replace w by ηw, where η is the effective proportion of the fuel raised to ignition temperature during the preheating process. Frandsen (1973) gives empirical values for η for several fuels used in laboratory fires. Thomas (1967) uses a physical argument to estimate η. Because we are currently working mainly with fine fuels, we use the thermally-thin approximation $\eta = 1$.

For a surface fuel element, putting $z = 0$ in (16) and integrating gives

$$R\rho_b Q_{\rm ig} = \int_0^\infty q(X)\,dX, \tag{20}$$

where $q(X) = q(X,0)$.

In the simplest models, equations (18) or (20) are used to determine the rate of spread R. In less simple models however, the rate of energy transfer q depends on the fuel temperature T, for example through the convective heating term (8). Then (18) and (20) are inappropriate; instead the differential equation (16) must be solved directly.

5. The physical model

From (16) and(17) we have

$$-R\rho_b c^* \frac{dT}{dX} = q_f(X, L, \phi_f) + q_i(X, \delta, \phi_i) - 4k_r\epsilon_p\alpha\sigma_B(T(X)^4 - T_\infty^4) + 4\alpha\hbar(X)(T_a(X) - T(X)), \tag{21}$$

where we have used (8) for the convective heating term, and have explicitly referred to the dependence of the radiative heating term q_f on the flame length L and flame angle ϕ_f, as well as on the distance from the fire front X.

The radiative loss term contains a factor k_r, to account for the fact that the surroundings of the surface fuel element are not completely at ambient temperature T_∞. If they were, then we would have $k_r = 1$. If we assume that the only heat loss is upwards, then $k_r = 0.5$. If the fuel close to the surface is close to the surface fuel temperature, then there will be comparatively little net radiative heat transfer downwards, and $k_r \approx 0.5$. Regardless, we have the bound $0.5 < k_r < 1$.

Equation (21) can be integrated directly to give

$$R\rho_b Q_{\text{ig}} = \int_0^\infty q_f(X)\,dX + \int_0^\infty q_i(X)\,dX - 4k_r\epsilon_p\alpha\sigma_B \int_0^\infty (T(X)^4 - T_\infty^4)dX + 4\alpha \int_0^\infty \hbar(X)(T_a(X) - T(X))\,dX \tag{22}$$

Note that this equation contains the unknown temperature field $T(X)$ on the right-hand side, and so cannot be used to find the rate of spread R, unless this temperature field is known or can be predicted.

6. Modelling the radiative heating

We considered four possible models for the absorption of radiation from the flame by the surface fuel element.

slab bed

In this model the fuel surface is assumed to be a solid surface, which absorbs radiation from the flame. The heat is transmitted down through the fuel by some unspecified mechanism to the rest of the bed. This model was used by Hottel et al. (1965), Van Wagner (1967) and Thomas (1967), amongst others. Regardless of the merits of this model (and we would argue that it is unrealistic for most naturally-occurring fuels, and also for our laboratory fuel beds), this is a whole-bed model, not a surface heating model.

modified slab bed

Here the radiation is assumed to be absorbed as though the fuel surface were solid, but the amount absorbed is multiplied by the factor α to allow for the porosity of the fuel bed. This model was used by Rothermel (1971). It is similar (but not equivalent) to the slab model with heat transfer assumed to be vertical radiation through the bed. It is equivalent to the volume heating model if the radiation impinges vertically onto the fuel bed surface.

volume heating

The radiation passes through the fuel bed, being absorbed at a rate of α per unit length, and so heating the fuel. Reflection is ignored — thus the fuel particles are assumed to behave approximately as black bodies. This model was used by Albini, (1985, 1986). Albini included an extra heat transfer term, re-radiation from warmed fuel particles, which we have ignored.

surface particle

Instead of a surface volume element, we can instead consider an energy balance for a single fuel particle on the fuel surface. The particle can be regarded as being randomly oriented, in which case the rate of spread would be calculated after taking the expectation over all directions, or, for special purposes, a particular orientation can be considered (see Appendix B).

For the slab bed model, with a flame of uniform emissive power, the rate of radiation being absorbed by an elemental area on the surface at X, per unit area of the surface, is given by $E_f J_f(X)$, where E_f is given by (5) and $J_f(X)$ is the view factor for two inclined rectangles. If the flame temperature and/or emissivity varies with height above the fuel bed, then the rate of radiation absorption can still be written in the same way, although $J_f(X)$ is no longer a view factor. The values of $J_f(X)$ for both cases are given in Appendix C. For the modified slab bed, the rate of radiation absorption is just $\alpha E_f J_f(X)$, with the same J_f as for the slab bed.

The rate of radiation absorption for the volume heating and single particle models can also be written in the form $\alpha E_f J_f(X)$. Appropriate formulæ for J_f are given in Appendix C.

The only physically self-sonsistent model for radiative heating from the combustion zone is that of volume heating, where the radiation passes through the semi-tranparent fuel, being gradually absorbed and heating the fuel as it progresses. We adopt the standard model, appropriate for a fuel bed of randomly-oriented black particles, and used as an

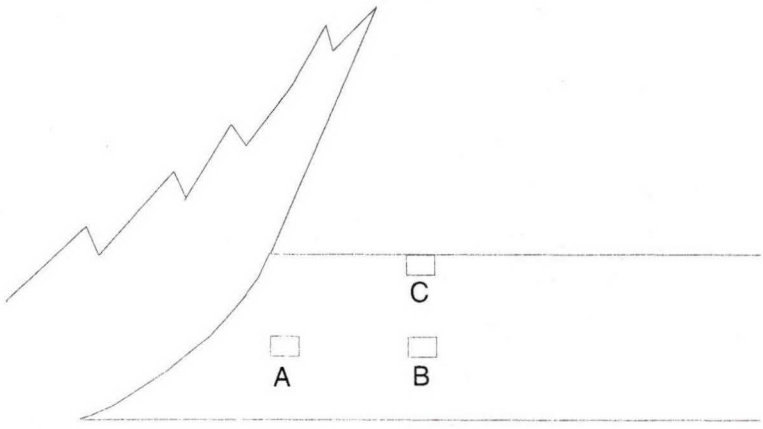

Figure 5. Fuel elements within the bed and on the fuel bed surface

approximation for other beds, that the radiation emanates from a solid interface between the unburnt and buring fuel zones, and decays exponentially as it passes through the bed, with mean free path length equal to $1/\alpha$. The radiative heating from the combustion can then be written, in a similar way to that from the flame, as $\alpha E_i J_i(X)$. Appropriate formulæ for J_i are given in Appendix D.

Choosing the volume-heating model for the flame radiation, the governing differential equation (21) for the fuel temperature becomes

$$-R\rho_b c^* \frac{dT}{dX} = \alpha\varepsilon_p\big(E_{f,0}J_f(X) + E_i J_i(X)\big) - 4k_r\epsilon_p\alpha\sigma_B(T(X)^4 - T_\infty^4) + 4\alpha\hbar(X)(T_a(X) - T(X))\,. \qquad (23)$$

7. Cold boundary condition

There are numerical difficulties with solving (23) for large X, since $J_f(X) = O(1/X)$ as $X \to \infty$ (see Appendix E), and so $\int_0^\infty J_f(X)\,dX = \infty$. This is a very similar problem to that found by Albini (1985), and the solution is the same: to use asymptotic approximation in (23) for large X, and to solve the resulting equation analytically. The result is that a location X_b can be found where the temperature has risen above ambient by a specified (small) amount θ_b, or equivalently, the temperature rise θ_b can be found for a given (large) distance X_b from the flame. The relations are derived in Appendix E.

8. Reason for choosing a surface fuel element

Figure 5 shows fuel elements within the fuel bed at B and (closer to the ignition interface) at A, and on the fuel bed surface at C. It is fairly clear that, compared with the surface

fuel element at C, the amount of radiation received at B depends to a greater extent on the combustion zone radiation and less on the flame radiation. The difference will be more pronounced closer to the flame at A. The radiation from the combustion zone depends heavily on the slope (and, more generally, the shape) of the interface, which is unknown and difficult to observe (and model). The radiation from the flame, on the other hand, depends on the flame height and angle, which are relatively easy to observe.

We have made the assumption that the combustion interface is straight, and at the same angle as the flame. Thus our model has no dependence on the combustion zone shape. This is reasonable for a surface fuel element, where the contribution from the combustion zone is less important than that from the flame, and comes mainly from the part of the combustion zone near the surface. But it would be an unreasonable assumption for a fuel elelment that is not near the surface, and so would also be inappropriate for a whole-bed element (see Figure 1c).

The above reasoning is valid for surface fires, such as the laboratory fires and forest litter fires. For crown fires, for example, the combustion zone radiation probably plays a larger part in the fire propagation, and we will need to check the application of the model specifically for such cases.

9. Instrumentation

A number of the terms in (23) need to be known before it can be used to find the spread rate R, including the radiative flux from the flame and combustion zone. The radiation from the flame to a point on the fuel bed surface might depend on the (vertical) height of the flame, the distance of the point from the flame, X, and the temperature of the surrounding gas T_a (a function of X). We measured these terms for many fires under different fuel and environmental conditions. Fuels used were regular excelsior (surface area to volume ratio 7596 m^{-1}), coarse excelsior (3092 m^{-1}), and Ponderosa pine needles (5710 m^{-1}). Details of the range of conditions and experimental setup are given in Catchpole et al. (1998). We will discuss modelling the terms in (23) in a later paper. Here we describe how the terms were obtained.

9.1 *Radiative flux from the flame*

Radiative flux from the flame was measured with narrow angle radiometers mounted at 5 different heights above the fuel bed, and pointing horizontally towards the flame. The radiometers had an acceptance angle of about 3°. They were mounted in a vertical bank in the centre of the fuel bed, 7 m from the end of the bed where the fire was ignited. Data was sampled at 20 Hz. An average value of the radiative flux was obtained from each

radiometer as described by Butler (1993). Average fluxes at each height from fires under the same fuel and environmental conditions were used to fit an equation relating radiative flux to the height of the radiometer. The basic equation was of the form

$$q(z/H) = q_{\max} \exp\left(-\left(\frac{z/H}{\sigma_G}\right)^2\right), \tag{24}$$

where z is the radiometer height, H is the flame height, and $q_{\max}$ and σ_G were determined separately for each set of fuel and environmental conditions.

9.2 *Radiative flux from the combustion zone*

Combustion zone radiation was set at 50 kW/sq m for Byram's intensity less than 250 kW/m, and 100 kW/sq m for Byram's intensity greater or equal to 250 kW/m, averages taken from a set of experiments with the narrow angle radiometer pointing at, and close to, the combustion zone.

9.3 *Air and fuel temperatures*

Fuel temperature was measured using a type K thermocouple (with 0.076 mm wire diameter) inserted into a small hole drilled through a piece of excelsior fuel. The excelsior fuel pieces used were 4 cm long, and as uniform in cross-section as possible. (In the case of Ponderosa pine needles the fuel thermocouple was threaded longitudinally through the center of the needle.) Another 0.076 mm thermocouple was placed as close as possible to the fuel thermocouple, without touching the fuel. There was generally about 1 mm between the air thermocouple and the fuel particle surface. Three pieces of fuel instrumented in this way were fastened at each end to parallel rods, thus forming a 'ladder' with rungs of fuel 15 cm apart. This was done to ensure the fuel did not curl as it decomposed, and so change its position with respect to the flame. The ladder was placed in the center of the fuel bed, 5 m from the end of the bed where the fire was ignited. Data from the thermocouples was sampled at 20 Hz.

The air and fuel temperatures from each temperature pair were plotted, and the thermocouple pair rejected if the traces indicated that the fuel thermocouple was tracking the air thermocouple too closely, indicating that the fuel thermocouple was too close to the fuel surface. As the temperature profiles from different rungs were quite variable, the traces from the rungs of each fire were averaged with the traces from all fires burned under the same fuel and environmental conditions. This was done by aligning the traces at the assumed ignition temperature of 593 K. The average profiles from one of these sets of conditions, consisting of 12 rungs from 5 fires, are shown in Figure 6. Thus the temperature data consisted of sets of air/fuel thermocouple profiles, each set corresponding to a unique

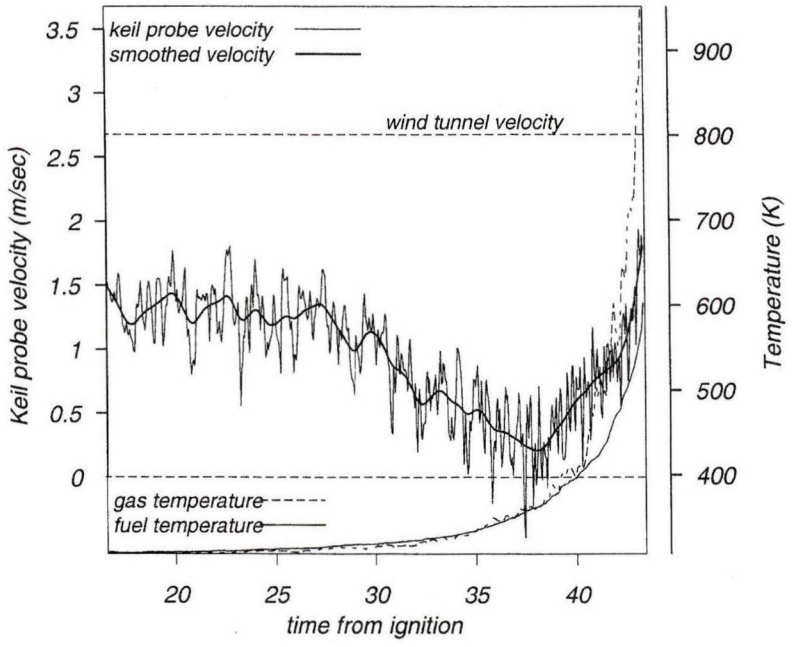

Figure 6. A typical graph of thermocouple measurements to determine fuel and air temperatures ahead of the spreading fire, from the ladders, and of the raw and smoothed air velocity as measured by the Keil probe.

set of conditions (fuel type, wind speed, moisture content, packing ratio, and fuel bed depth).

9.4 *Gas flow*

To measure surface wind velocity we used a Keil probe (McCaffrey and Heskestad, 1976). The probe had in input diameter of 12.7 mm, and an acceptance angle of $\pm 30°$. The probe was placed horizontally on the fuel surface close to the second rung of the thermocouple ladder, facing the flame front. On some fires there were additional probes, one pointing vertically upwards, and one pointing towards the side of the wind tunnel. Pressure readings from the probes were converted to velocity, using Bernoulli's equation, correcting for changes in air density with changing temperature, using a thermocouple near the probe opening. A typical velocity profile from a forward facing probe is shown in Figure 6.

To decompose the velocity into an average velocity and deviations from the average (which relate to the turbulence), a smoother was fitted to the data to give an estimate of average flow (see Figure 6), and the sum of squared deviations from the smoothed value was calculated. The Keil-probe readings were smoothed with a robust local smoother,

smoothing 5% of the data at each point (see Cleveland, 1985). Smoothed traces from fires in the same fuel and environmental conditions were averaged using a similar process to the thermocouple averaging. Estimates of velocity deviations were also averaged.

It can be seen from Figure 6 that the average gas flow at the surface is around half of the tunnel wind speed until just before the fire arrives. There is then a drop in gas velocity in the low pressure region just ahead of the fire. In low wind speed, medium-to-high intensity fires, this is often seen as a reversal of velocity, giving an inflow into the fire. The velocity then rises rapidly to wind tunnel velocity. A full analysis of the velocity data will be given in a future paper.

10. Matching the temperature profiles

If all the terms in (21) except the fuel temperature are known, we can predict the fuel temperature at any point X by (21), and compare our predictions with the observed fuel temperature profile obtained from the fuel thermocouple. In fact, the fuel emissivity and the heat transfer coefficient are also unknown. Data given in Jarvis et al. (1976) indicates that fuel particle emissivities for wildland vegetation range from 0.70 to 1 (black body assumption). We took the emissivity of excelsior to be 0.75, and the emissivity of pine needles to be 0.85.

Note that when the emissivity is less than one, there will be internal reflection of radiation in the fuel bed. We neglect this.

For the Reynolds-Nusselt relationship we used the formula (9) for a cylinder in a cross-flow from Incropera and De Witt (1990, eqn. 7.56). The film temperature was set at 300°K up to the time where the temperature rose steeply in the presence of hot gases from the flame. In this latter region it was set as 600°K. The smoothed values of the Keil probe were used to determine the Reynolds number at a distance X from the fire front.

11. Correcting the air thermocouple for radiation

Experiments comparing the temperature profiles for aspirated and non-aspirated thermocouples showed that bare thermocouples tend to record higher temperatures than aspirated thermocouples, showing that even the 0.076 mm diameter air thermocouples used are affected by radiation from the flame. It was not possible to shield the air thermocouple, as we required that the air and fuel thermocouples be as close as possible, and in any case shielding changes the fluid boundary layer around the thermocouple. We chose to correct the air thermocouple for the effect of radiation, using an energy balance similar to (21). We assumed the thermocouple to be in thermal equilibrium, so that $\frac{dT_{tc}}{dt} = 0$. In other words the thermocouple reacts much faster than the fuel to changes in the gas temperature. This

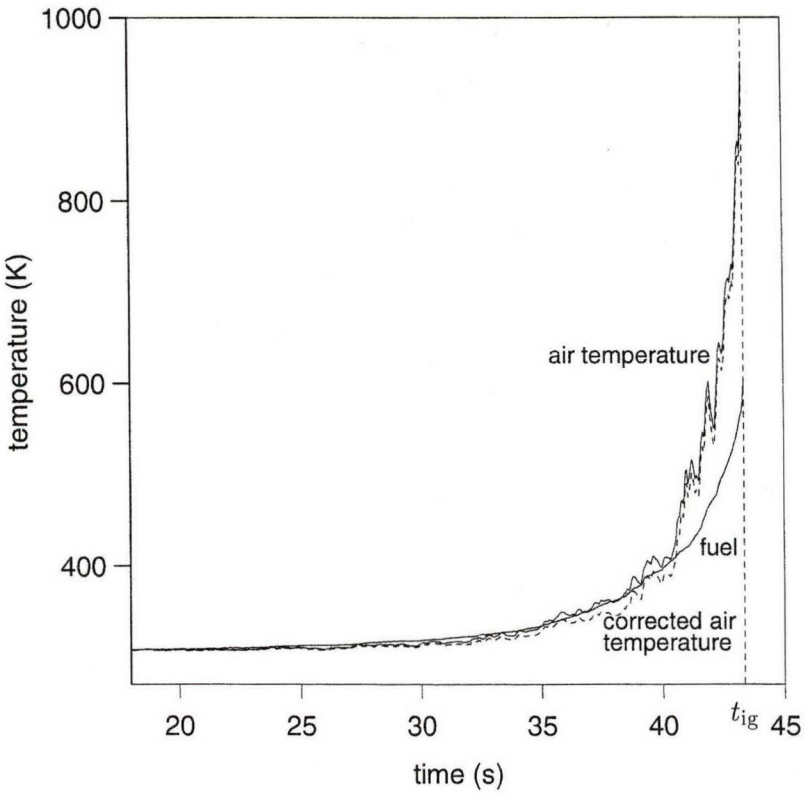

Figure 7. The temperature traces from the air and fuel thermocouples, and the corrected air temperature after allowing for radiative heating of the air thermocouple.

gives an equation for the true air temperature (see Shaddix, 1999, eqn. (3)).

We took the emissivity of the thermocouple to be 0.65 (Hottel and Sarofim, 1967). The type K thermocouple is comprised of a solder bead of diameter about 0.109 mm, and bare wire of diameter 0.076 mm. As the bead is only a small fraction of the thermocouple junction, we assumed an approximate cylindrical shape of diameter 0.076 mm, and used the same Reynolds-Nusselt relationship as for the fuel. The Reynolds-Nusselt correlation proposed by Shaddix (1999) yields very similar results. To avoid problems with the correction when the surface velocity was zero the surface velocity was set at 0.01 m/s when the absolute value measured by the Keil probe was less than 0.01 m/s. This corresponds approximately to assuming free convection when the surface velocity was less than 0.01 m/s.

We thus could obtain an estimate of the true air temperature. The air temperature and corrected air temperature are shown in Figure 7. The correction is not large for a fire such as this, at a windspeed of 2.7 m/sec.

12. Matching the fuel temperature profile

We consider first matching the average temperature profile from a set of data comprised of 12 rungs from 5 fires under the same fuel and environmental conditions, shown in Figure 6. For this set of fires in coarse excelsior ($s = 3092\,\mathrm{m}^{-1}$), the fuel packing ratio was $\beta = 0.01$, the fuel depth was 0.15 m, the tunnel windspeed was 2.68 m/sec, and the average moisture content was 6%. The average spread rate, flame height and flame angle were 0.112 m/sec, 1.15 m and 39° respectively. The fuel density was $398\,\mathrm{kg/m}^3$, giving $\rho_b = 3.98\,\mathrm{kg/m}^3$. To determine c^* from (4) we need to fix an ignition temperature. Examination of traces of several fires suggested that 593°K was reasonable (see also Anderson, 1969). For coarse excelsior this then determines $Q_f = 504\,\mathrm{kJ/kg}$ from integration of Susott's (1982) DSG curves, (*need to fix 1.3 to reflect this*) and gives $c^* = 2.10\,\mathrm{kJ/kg/°K}$. Average radiometer data from these fires gave $q_{\max} = 105\,\mathrm{kW/sq\ m}$ and $\sigma_G = 0.26$ in (24).

Solving the differential equation (21) numerically then gives a predicted fuel temperature which can be compared with the measured fuel temperature. The result was that fuel temperature was badly overestimated, indicating that the right hand side of (21) was too large (see Figure 8). This could be fixed by lowering the fual particle emissivity to less than the value of 0.75 used, but this seems unreasonable (Jarvis et al., 1976). The Reynolds-Nusselt correlation used, however, which are derived from experiments with laminar flow of warm air, could easily be inappropriate for turbulent flow of incandescent gas. Using trial and error for a range of fire sets we varied the heat transfer coefficient, somewhat naively, by multiplying by a constant to see whether a different correlation might be appropriate. High values of $\hbar$ and $\bar{h}_{tc}$ often badly overestimated the fuel temperature, low values of $\hbar$ and $\bar{h}_{tc}$ could give predicted air temperatures below ambient.

It is reasonable to conjecture a different heat transfer coefficient in the two regions. In the high temperature region the fuel particle is decomposing, and mass transfer from the volatiles and cellulose breakdown could affect the boundary layer, reducing the heat transfer rate. We tried reducing $\hbar$ in the region close to the fire. This was unsatisfactory for many of the fires as it required the predicted air temperature to drop too low before the fuel temperature close to the flame front could be matched. The predicted fuel temperatures also tended to be non-smooth.

We then considered whether the radiative flux might be overestimated by our measurements.

13. Radiative flux overestimation

The radiative flux from the base radiometer should be related to the gas temperature at the base of the flame, which we could measure from the air/fuel thermocouple pair. Note

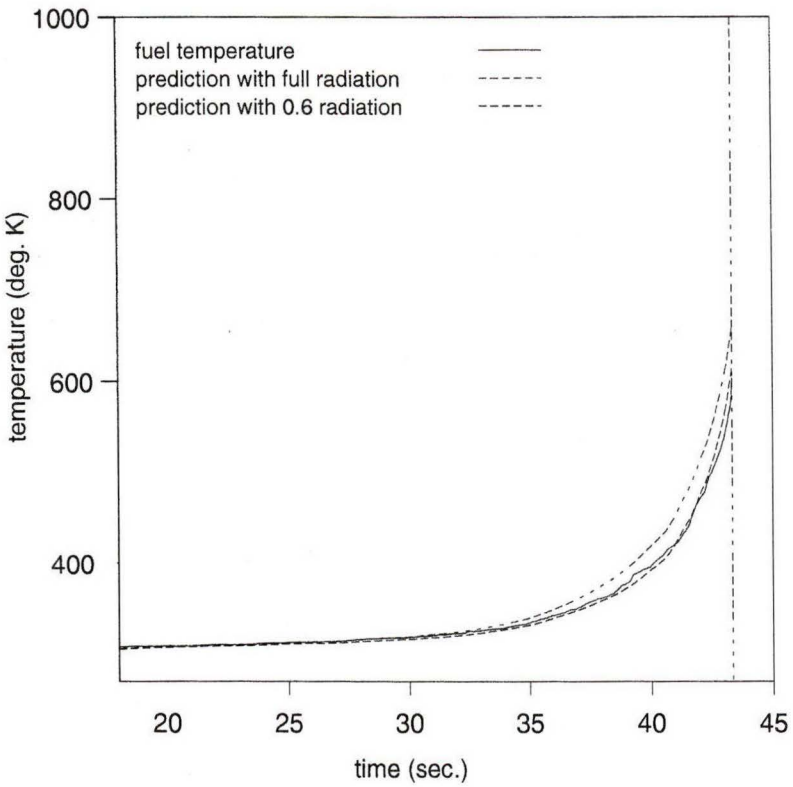
1000
800
600
400
temperature (deg. K)
fuel temperature
prediction with full radiation
prediction with 0.6 radiation
20
25
30
35
40
45
time (sec.)

Figure 8.

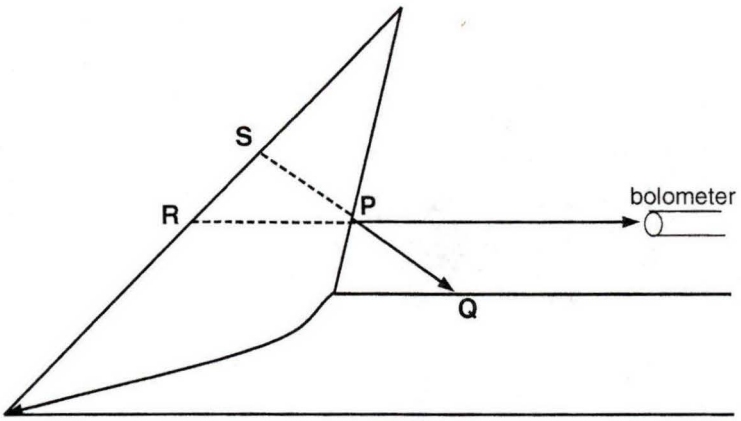

Figure 9. Radiation from a diffuse flame

that no correction for radiation is required when the thermocouple is bathed in the flame. The gas temperature fluctuates through the flame due to turbulence causing pockets of cooler air. The radiative flux should approximate to (5) with $\epsilon_f = 1$ for a thick flame. The air thermocouple for the set of fires in question gave an average value corresponding to $\sigma_B T_a^4 = 61\,\mathrm{kW/m^{-1}}$, whereas the base radiometer average reading was $104\,\mathrm{kW/m^{-1}}$, a reduction factor of 0.6. It is possible that this was because the base radiometer is viewing some radiation from the dense glowing particles in the combustion zone.

There is also the possibility of overestimating the radiative flux reaching the fuel particles because of the assumption of the flame as a flat radiating surface. The radiative flux from any point P on the flame (see Figure 9) is measured from the radiometer at height h which points horizontally at the flame. It is a function of the temperature and carbon density along a horizontal line through the flame at height h. In the calculation of radiative flux onto the fuel particles, point P is used as though it were a point on a flat plate radiating with intensity q_h which is determined from the radiometer at height h. Consider however the radiative flux from point P to point Q on the fuel surface. The radiation is in fact coming from the carbon particles on the dashed line PS through the flame, and will tend to be lower than that from the horizontal path PR, because the particle density is less higher in the flame and the gas temperature is lower. This generally causes an overestimation of the radiative flux from P to the fuel, particularly close to the flame. Without a full 3-dimensional flame temperature and carbon density model it is impossible to quantify the overestimation. Experiments using radiometers inclined upwards failed to provide good estimates of the effect.

Another possible explanation for the overestimate of the radiation is that radiation

from flame to fuel particle (particularly near close to the flame) may be attenuated by water vapour. Radiation from the flame to the bolometers would also be attenuated, but not to the same extent.

We introduced a radiative reduction factor to account for this possible overestimation of the flame radiation. A radiation reduction factor of 0.6 gave reasonable results for coarse excelsior fires, although temperature profiles for fires in pine needles and regular excelsior with higher packing ratios were still overestimated.

14. Fitting the temperature profiles of all data sets

With a radiation reduction factor of 0.6 the standard Reynolds-Nusselt correlations for the fuel and thermocouple convective heat transfer coefficients gave a good prediction of the fuel temperature for the set of fires in Figure 6. The predicted fuel temperature profile is shown in Figure 8.

A 'pseudo-prediction' of spread rate $\widehat{R}$ can be determined which gives an indication of how well the model predicts ignition time. Since the observed spread rate R_{obs} is input into (21) it is not a real prediction. The pseudo-prediction can be calculated from

$$\widehat{R} = \frac{R_{obs}(\hat{T}_0 - T_\infty)}{T_{\text{ig}} - T_\infty}, \tag{25}$$

where $\hat{T}_0$ is the fitted temperature when the observed fuel temperature is at ignition temperature ($T_{\text{ig}} = 593°\text{K}$), and T_∞ is ambient temperature. The pseudo-predictions for the coarse excelsior fires for which we had radiative flux estimates and surface velocity profiles are shown plotted against the observed values in Figure 10. There is quite a bit of scatter, but the predictions are centered around the line of perfect fit.

15. A true predictive model

The model used to provide pseudo-predictions cannot be used to predict spread rates as it contains several terms that are unknown prior to the fire. These include flame length, angle, radiative flux, air temperature profile and surface wind velocity. Submodelling these unknown terms, and the determining the resulting spread rate predictions, is discussed in Part 2 of this Report.

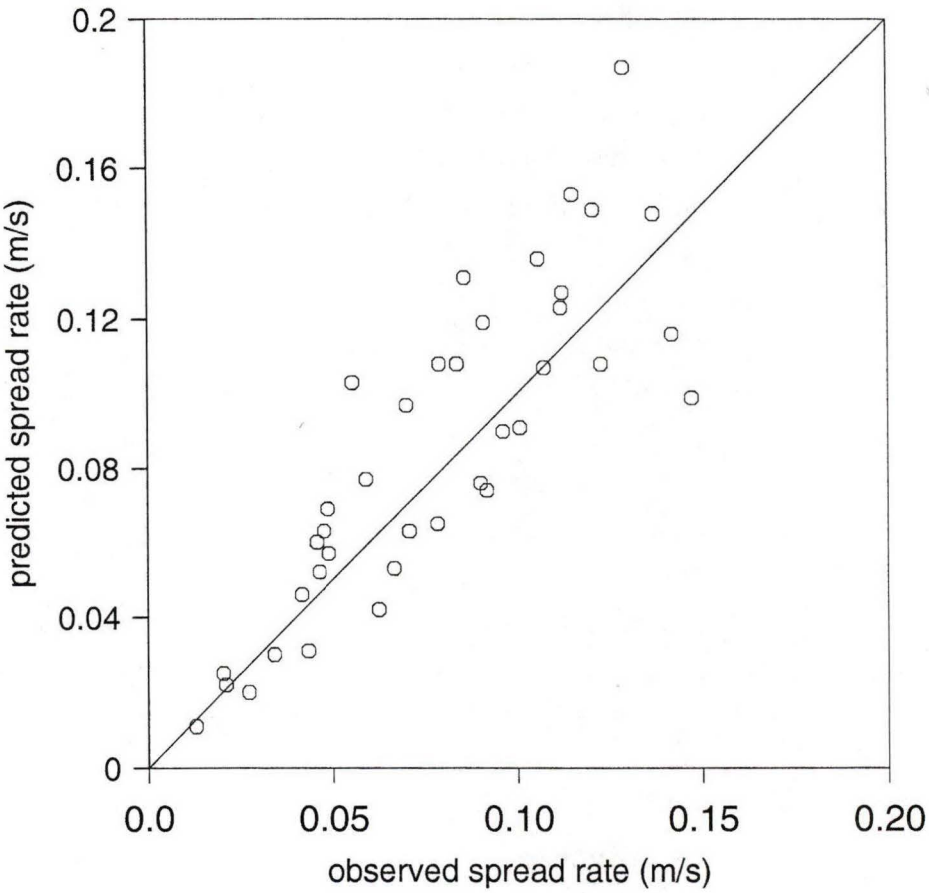
0.2
0.16
0.12
0.08
0.04
0
predicted spread rate (m/s)
0.0
0.05
0.10
0.15
0.20
observed spread rate (m/s)

Figure 10.

Appendix A

Glossary of notation

$\alpha = s\beta/4$	decay constant for radiation through the fuel bed
β	packing ratio of fuel bed = volume of fuel per unit volume of fuel bed
ϵ_b	combustion interface emissivity
ϵ_f	flame emissivity
η	the effective fraction of the fuel raised to ignition temperature during the preheating process
ϕ_f	flame angle to vertical
ν	kinematic viscosity of gas (air)
$\rho_b = \beta\rho_p$	bulk density of fuel = mass of fuel per unit volume of fuel bed
ρ_p	density of a single fuel particle
σ_B	Stefan-Boltzman constant
b	effective flame height multiplier
c_p	specific heat of dry fuel
c_w	specific heat of water
c^*	'average specific heat' of fuel
D_f	flame depth at base of flame
$E_f = \epsilon_f\sigma_B T_f^4$	flame emissive power
F_r	Froude number
h	the depth of the fuel bed
$\hbar$	convective heat transfer coefficient
h_c	fuel low heat content
H_f	flame height
I_B	fireline intensity
$I_P = R\rho_b\eta Q_{\text{ig}}$	propagating flux
k	thermal conductivity of gas (air)
L_f	flame length
L_c	convection length
$\mathcal{L}$	latent heat of water
m	moisture content of fuel = mass of water per unit mass of fuel
$N_u = \hbar L/k$	Nusselt number
q	rate of heat inflow into unit volume of the fuel bed
q_i	radiative heating rate from the combustion (ember) interface
q_c	convective heating rate

q_f	radiative heating rate from the flames
q_ℓ	cooling rate
Q	quantity of heat per unit mass of fuel
Q_f	quantity of heat required to raise unit mass of dry fuel to ignition temperature
Q_{ig}	quantity of heat required to raise unit dry mass of moist fuel to ignition temperature
$R_e = U_0 L/\nu$	Reynolds number
s	surface area to volume ratio of a single fuel particle
$S_f = L \sin \phi_f$	flame shadow
T	fuel particle temperature
T_f	flame temperature
T_{ig}	Ignition temperature
T_∞	ambient temperature
U	wind speed
U_0	wind speed at surface of or within fuel bed
$w = \rho_b h$	total fuel loading per unit area of the fuel bed
w_a	actual fuel load consumed during combustion

Appendix B

Energy balance for a single particle

We derive here the rate of radiation from the flame absorbed by a single particle on the fuel surface. We assume that the particle is cylindrical and oriented horizontally, directly across the fuel bed: that is, parallel to the flame (see figure 11). This orientation is of special interest because the instrumented pine needles were oriented in this way. However it is a simple matter to redo the calculation for any other orientation.

We use a coordinate system (X, y, z) moving with the flame, whose origin is at the base of the flame and, in the case of a finite-width flame, at the centre of the flame. The fuel particle is located on the fuel surface a distance X ahead of the flame, at point Q with position vector $(X, 0, 0)$. We consider a ray, from a point $P = (z \tan \phi_f, y, z)$ on the flame surface at height z above the fuel bed, onto the particle. First note that

$$\vec{PQ} = (X - z \tan \phi_f, -y, -z)$$

and that the unit normal to the flame at P is

$$\mathbf{n} = (\cos \phi_f, 0, -\sin \phi_f),$$

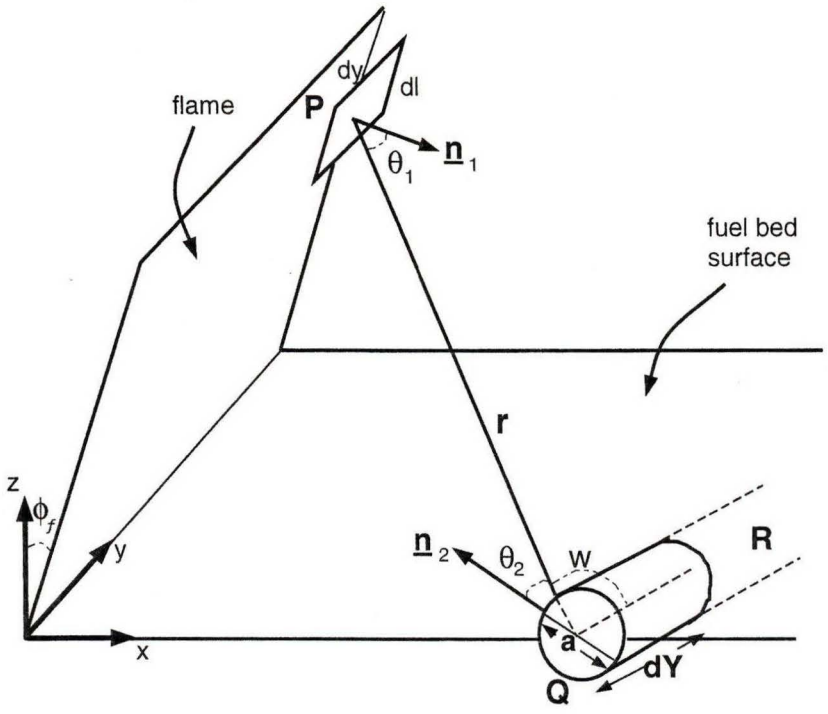

Figure 11. Radiation from the flame onto a single particle.

and so the angle θ_1 between the ray and the normal satisfies

$$\begin{aligned}\cos\theta_1 &= \frac{\mathbf{n}.\vec{PQ}}{\|\vec{PQ}\|} \\ &= \frac{(X - z\tan\phi_f)\cos\phi_f + z\sin\phi_f}{r} = \frac{X\cos\phi_f}{r},\end{aligned}$$

where

$$r = \|\vec{PQ}\| = \sqrt{(X - z\tan\phi_f)^2 + y^2 + z^2}.$$

The unit vector along the particle is $\vec{QR} = (0, 1, 0)$, and so the angle ω between the ray and the particle satisfies

$$\cos\omega = \frac{\vec{QP}.\vec{QR}}{\|\vec{QP}\|} = \frac{y}{r}.$$

Hence the angle θ_2 between the ray and the normal plane to the particle satisfies

$$\cos\theta_2 = \sin\omega = \frac{\sqrt{(X - z\tan\phi_f)^2 + z^2}}{r}.$$

Now consider a length dY of the particle at Q. The area of this segment, as seen from P, is $adY\cos\theta_2$, where a is the diameter of the cylinder. Hence the solid angle subtended at P is $adY\cos\theta_2/r^2$.

The intensity of radiation emitted per unit solid angle from a small element dA of the flame surface at P, in the direction $\vec{PQ}$, is

$$dI = \frac{E_f}{\pi} dA \cos\theta_1,$$

where $E_f = \sigma_B \epsilon_f T_f^4$ is the hemispherical flame emissive power at the point P, which in general will depend on the height z. Writing $dA = dy\,d\ell = dy\,dz/\cos\phi_f$, where $d\ell$ is measured along the flame (see figure 11), this becomes

$$dI = \frac{E_f}{\pi} \cos\theta_1 \frac{dy\,dz}{\cos\phi_f}.$$

The particles aborb a fraction ε_p of the radiation incident upon them, and so the rate of absorption of radiation by the particle element at Q, from the flame element at P, is

$$\begin{aligned} dQ &= \varepsilon_p \frac{E_f}{\pi} \cos\theta_1 \frac{dy\,dz}{\cos\phi_f} \frac{adY\cos\theta_2}{r^2} \\ &= \varepsilon_p \frac{E_f}{\pi} \frac{X\cos\phi_f}{r} \frac{dy\,dz}{\cos\phi_f} \frac{adY}{r^2} \frac{\sqrt{(X - z\tan\phi_f)^2 + z^2}}{r}. \end{aligned}$$

Hence the rate of absorption of radiation from the flame, per unit length of the particle, is $a\varepsilon_p E_{f,0} J_f(X)$, where $E_{f,0}$ is the flame emissive power at the base of the flame, and

$$J_f(X) = \frac{X}{\pi} \int_{z=0}^{H} \frac{E_f(z)}{E_{f,0}} \int_{y=-W}^{W} \frac{\sqrt{(X - z\tan\phi_f)^2 + z^2}}{r^4} dy\,dz,$$

where $r^2 = (X - z\tan\phi_f)^2 + y^2 + z^2 = c^2 + y^2$ say, and the flame is taken to be of height H and of width $2W$. The innermost integral is

$$\int_{y=-W}^{W} \frac{c}{(c^2+y^2)^2} dy = \frac{1}{c^2}\left\{\arctan\left(\frac{W}{c}\right) + \frac{cW}{c^2+W^2}\right\}.$$

Hence

$$J_f(X) = \frac{X}{\pi} \int_{z=0}^{H} \frac{E_f(z)}{E_{f,0}} \frac{1}{c^2}\left\{\arctan\left(\frac{W}{c}\right) + \frac{cW}{c^2+W^2}\right\} dz, \tag{B.1}$$

where $c^2 = (X - z\tan\phi_f)^2 + z^2$.

We now apply the conservation of energy to a unit length of the fuel particle, to derive the fundamental differential equation analagous to equation (21). First note that the

volume of this segment is $\pi a^2/4$, and its surface area is πa. As before, we assume that only a fraction η of the particle is involved in the preheating process. The equation is thus

$$-R\frac{\pi a^2}{4}\rho_p \eta c^* \frac{dT}{dX} = a\varepsilon_p E_{f,0} J_f(X) + \pi a \hbar(X)\Big(T_a(X) - T(X)\Big). \tag{B.2}$$

This can be rewritten in terms of the particle's surface-area to volume ratio $s = 4/a$ as

$$-R\rho_p \eta c^* \frac{dT}{dX} = s\,\varepsilon_p \frac{E_{f,0}}{\pi} J_f(X) + s\hbar(X)\Big(T_a(X) - T(X)\Big). \tag{B.3}$$

Note that this equation is very similar to (21). The similarity is more apparent if we divide throughout (21) by the packing ratio β to obtain

$$-R\rho_p \eta c^* \frac{dT}{dX} = \beta^{-1} q_f(X, L, \phi_f) + s\hbar(X)(T_a(X) - T(X)). \tag{B.4}$$

It is clear that the difference, if any, resides solely in the radiative heating term q_f. Expressions for q_f for the various fuel bed models are derived in Appendix C.

Appendix C

Radiation absorption at the fuel surface

C1. Slab bed and modified slab bed

We consider the same situation as in Appendix B, except that here the fuel bed surface is modelled as a solid. Thus we consider the radiation from an element dA_1 at P on the flame surface to an element dA_2 at Q on the fuel bed surface (see figure 12).

From standard theory (see e.g Siegel and Howell equation 7.77), the rate of radiative transfer is

$$dQ = \varepsilon_p \frac{E_f}{\pi} \frac{\cos\theta_1 \cos\theta_2}{r^2} dA_1 dA_2, \tag{C.1}$$

where θ_1 and θ_2 are the angles between the ray $\vec{PQ}$ and the normals to the surfaces. From figure 12 we have that $\vec{PQ} = (X - z\tan\phi_f, -y, -z)$, and the normal to the flame surface is $\mathbf{n}_1 = (\cos\phi_f, 0, -\sin\phi_f)$, as in Appendix B, so that

$$\cos\theta_1 = \frac{X\cos\phi_f}{r},$$

where

$$r = \|\vec{PQ}\| = \sqrt{(X - z\tan\phi_f)^2 + y^2 + z^2}.$$

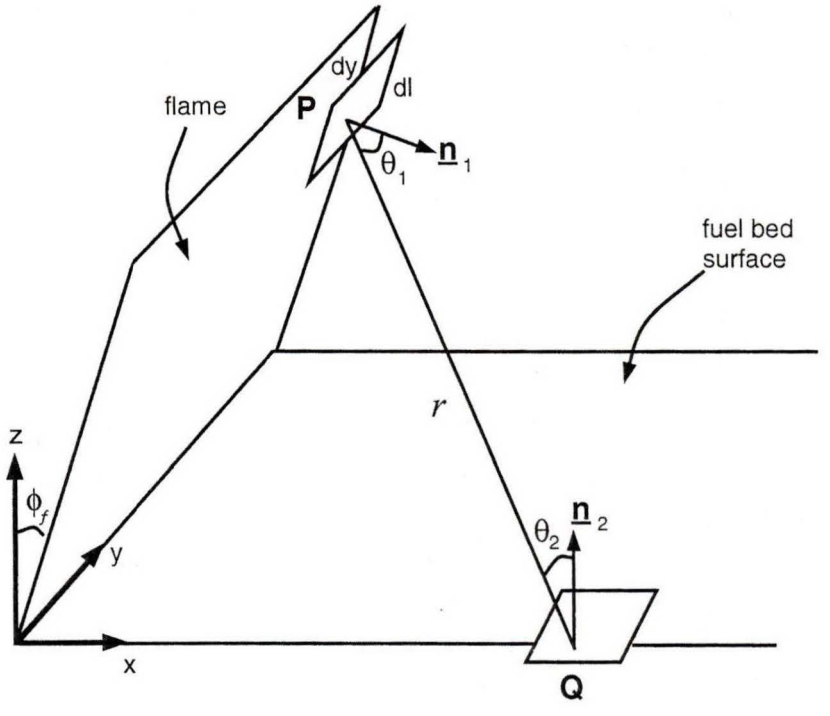

Figure 12. Radiation from the flame to the fuel bed surface.

Also the normal to the fuel bed surface is $\mathbf{n}_2 = (0, 0, 1)$, and so

$$\cos\theta_2 = \frac{\mathbf{n}_2.\vec{QP}}{r} = \frac{z}{r}.$$

As in Appendix B, $dA_1 = dy\,dz/\cos\phi_f$, and so the rate of radiation from dA_1 which is absorbed by the fuel bed at Q, is

$$dQ = \varepsilon_p \frac{E_f}{\pi} \frac{(X\cos\phi_f/r)(z/r)}{r^2} \frac{dy\,dz}{\cos\phi_f} = \varepsilon_p \frac{E_f}{\pi} \frac{Xz}{r^4} dy\,dz$$

per unit surface area of the fuel bed. Hence the rate of absorption,per unit surface area of the fuel bed, of the total radiation from a horizontal strip on the flame surface, at height z above the fuel bed and of width $d\ell = dz/\cos\phi_f$, is

$$\int_{y=-W}^{W} dQ = \varepsilon_p \frac{E_f}{\pi} Xz \int_{y=-W}^{W} \frac{dy}{r^4}\,dz = \varepsilon_p \frac{E_f}{\pi} \frac{Xz}{c^3} \left\{ \arctan\left(\frac{W}{c}\right) + \frac{cW}{c^2+W^2} \right\} dz,$$

where $c = \sqrt{(X - z\tan\phi_f)^2 + z^2}$. Hence the total radiative flux falling on the fuel bed surface at Q is $\varepsilon_p E_{f,0} J_f(X)$, where

$$J_f(X) = \frac{X}{\pi} \int_{z=0}^{H} \frac{E_f(z)}{E_{f,0}} \frac{z}{c^3} \left\{ \arctan\left(\frac{W}{c}\right) + \frac{cW}{c^2+W^2} \right\} dz. \qquad \text{(C.2)}$$

In the special case where the flame temperature and emissivity are assumed constant over the whole flame surface, $J_f(X)$ is the view factor between the flame surface and dA_2. From Hamilton and Morgan (1952), we have

$$J_f(X) = \frac{1}{\pi}\left\{\frac{W\sin\phi_f}{V_2}\left[\arctan\left(\frac{L-X\sin\phi_f}{V_2}\right)+\arctan\left(\frac{X\sin\phi_f}{V_2}\right)\right]+ \right.$$
$$\left. + \arctan\left(\frac{W}{X}\right) - \frac{X-L\sin\phi_f}{V_1}\arctan\left(\frac{W}{V_1}\right)\right\} \qquad \text{(C.3)}$$

where

$$V_1 = \sqrt{(X-L\sin\phi_f)^2+(L\cos\phi_f)^2}, \qquad V_2 = \sqrt{W^2+(X\cos\phi_f)^2}.$$

Note that for an infinitely wide fire front ($W \to \infty$), then, in general we get from (C.2)

$$J_f(X) = \frac{X}{2}\int_{z=0}^{H}\frac{E_f(z)}{E_{f,0}}\frac{z}{c^3}\,dz \qquad \text{(C.4)}$$

while for a constant temperature flame we get from (C.3) or (C.4)

$$J_f(X) = \frac{1}{2}\left(1-\frac{X-L\sin\phi_f}{V_1}\right). \qquad \text{(C.5)}$$

For the modified slab bed model, we assume that rate of radiation absorption by a volume element on the fuel bed surface, of top surface area dA_2 and thickness dz, is equal to αdz times the radiation falling on dA_2. This gives a rate of radiation absorption per unit volume of fuel bed as

$$q_f(X) = \alpha\varepsilon_p E_{f,0} J_f(X), \qquad \text{(C.6)}$$

where $J_f(X)$ is given by one of the above equations.

C2. Volume heating

The fuel bed is modelled as a collection of randomly oriented particles. Reflection from the particles, whicj occurs if the particle emissivity $\varepsilon_p < 1$, is ignored. Consider a beam of radiation from a small region dA_1 on the flame surface to a small cylindrical volume element on the surface of this bed (see figure 13). The rate of radiation from dA_1 falling onto this volume is

$$dI = \frac{E_f}{\pi}\frac{\cos\theta_1}{r^2}\,dA_1\,dA_2$$

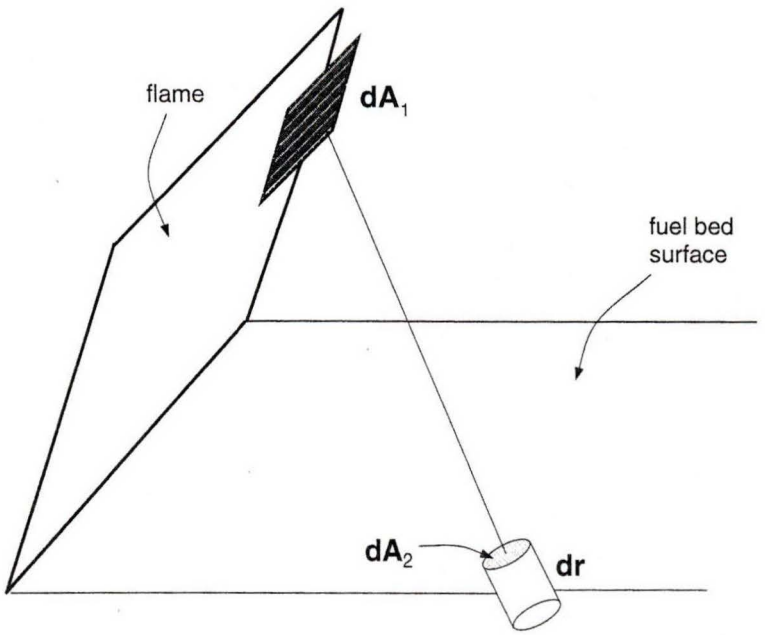

Figure 13. Radiation from the flame to a volume element on the fuel bed surface.

as in (C.1). Each ray in this beam will meet a fuel particle and be absorbed with probability $\alpha\varepsilon_p dr$, where[1] $\alpha = s\beta/4$, and so the rate of radiative energy absorbed by the volume element is

$$dQ = \alpha\varepsilon_p \, dI \, dr = \alpha\varepsilon_p \frac{E_f}{\pi} \frac{\cos\theta_1}{r^2} \, dA_1 \, dV,$$

where $dV = dA_2 \, dr$ is the volume of the fuel element.

Thus the rate of energy absorbed by the fuel bed, per unit volume of fuel bed, from the flame element dA_1 is

$$\frac{dQ}{dV} = \alpha\varepsilon_p \frac{E_f}{\pi} \frac{X \cos\phi_f}{r^3} \, dA_1 = \alpha \frac{E_f}{\pi} \frac{X}{r^3} \, dy \, dz.$$

Thus the total rate of radiative energy from the flame, absorbed per unit volume of the fuel bed, is $\alpha\varepsilon_p E_{f,0} \, J_f(X)$, where

$$\begin{aligned} J_f(X) &= \frac{X}{\pi} \int_{z=0}^{H} \frac{E_f(z)}{E_{f,0}} \int_{y=-W}^{W} \frac{dy}{r^3} \, dz \\ &= \frac{2XW}{\pi^2} \int_{z=0}^{H} \frac{E_f(z)}{E_{f,0}} \frac{dz}{c^2\sqrt{c^2+W^2}}, \end{aligned} \tag{C.1}$$

[1]This equation is correct for convex fuel particles. We ignore the small error for non-convex particles.

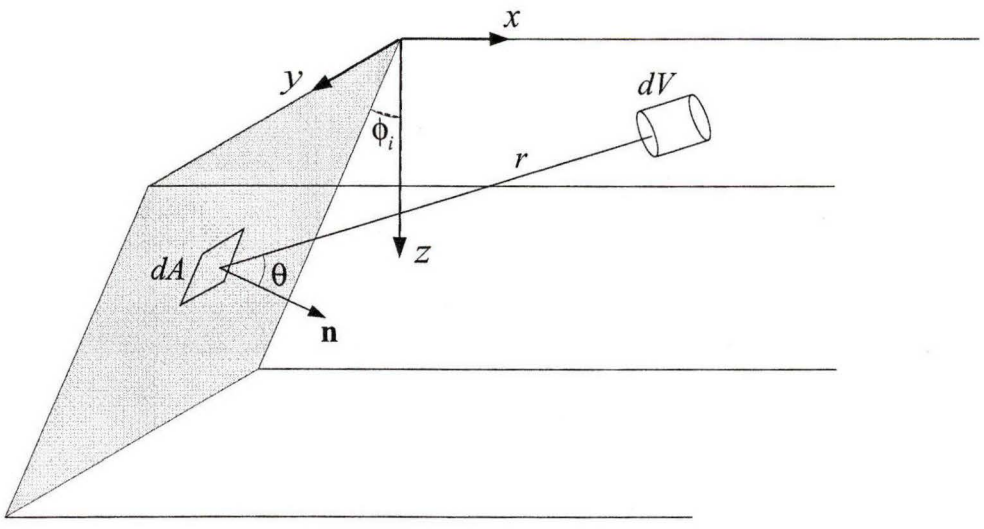

Figure 14. Radiation from the combustion interface to a fuel surface element

where

$$c^2 = (X - z\tan\phi_f)^2 + z^2.$$

In the special case where E_f is constant over the flame surface this reduces to

$$J_f(X) = \frac{2}{\pi}\left\{\arctan\left(\frac{W(L - X\sin\phi_f)}{X\cos\phi_f\sqrt{(L\cos\phi_f)^2 + W^2 + (X - L\sin\phi_f)^2}}\right) + \arctan\left(\frac{W\tan\phi_f}{\sqrt{W^2 + X^2}}\right)\right\}. \tag{C.2}$$

A special case of this formula, with $\phi_f = 0$, was given in de Mestre *et al* (1989).

Appendix D

Combustion zone radiation

We model the combustion interface as a plane, inclined at an angle ϕ_i to the vertical, as shown in Figure 14, and radiating as a solid surface at a hemispherical intensity of E_i. We consider an element dA on the interface, with position coordinates

$$(x, y, z) = (-z\tan\phi_i,\ y,\ z)$$

and a volume element dV on the surface, with position coordinates $(X,\ Y,\ 0)$. The radiation from dA absorbed by dV is then

$$dQ = \alpha\varepsilon_p\frac{E_i}{\pi}\frac{\cos\theta}{r^2}e^{-\alpha r}dA\,dV\,,$$

where $r = \sqrt{(X + z\tan\phi_i)^2 + (Y - y)^2 + z^2}$ is the distance of dV from dA. This is similar to the flame radiation (volume heating) case, the extra factor $e^{-\alpha r}$ occurring because this fraction of the radiation from dA will have already been intercepted by the fuel.

It follows, in the same way as in Appendix C, that the rate of energy absorbed per unit volume of the bed is

$$\frac{dQ}{dV} = \alpha\varepsilon_p \frac{E_i}{\pi}\frac{X}{r^3}e^{-\alpha r}\,dy\,dz$$

The total rate of absorption from the whole combustion interface, per unit volume of fuel bed, can thus be written as $\alpha\varepsilon_p E_i J_i(X,Y)$, where

$$J_i(X,Y) = \frac{X}{\pi}\int_{z=0}^{\delta}\int_{y=-W}^{W}\frac{e^{-\alpha r}}{r^3}\,dy\,dz\,, \tag{D.3}$$

where we have assumed that the radiation is uniform over the interface. At this stage we make the approximation that the combustion interface is infinitely wide. This will be a good approximation provided that the bed half-width $W$is reasonably large (> 2, say) compared with the mean free path length of radiation through the fuel, which is $1/\alpha$. Then (D.3) becomes

$$J_i(X) = \frac{2X}{\pi}\int_{z=0}^{\delta}\int_{y=0}^{\infty}\frac{e^{-\alpha r}}{r^3}\,dy\,dz \tag{D.4}$$

where $r = \sqrt{(X + z\tan\phi_i)^2 + y^2 + z^2}$. Now let

$$\rho = \sqrt{(X + z\tan\phi_i)^2 + z^2}$$

and define ψ by

$$y = \rho\tan\psi$$

so that

$$r = \sqrt{\rho^2 + y^2} = \rho\sec\psi\,.$$

Then the integral (D.4) becomes

$$\begin{aligned} J_i(X) &= \frac{2X}{\pi}\int_{z=0}^{\delta}\int_{\psi=0}^{\pi/2}\frac{e^{-\alpha\rho\sec\psi}}{(\rho\sec\psi)^3}\rho\sec^2\psi\,d\psi\,dz \\ &= \frac{2X}{\pi}\int_{z=0}^{\delta}\frac{1}{\rho^2}\int_{\psi=0}^{\pi/2}\cos\psi e^{-\alpha\rho\sec\psi}\,d\psi\,dz \\ &= \frac{2X}{\pi}\int_{z=0}^{\delta}\frac{e^{-\alpha\rho}}{\rho^2}A(\alpha\rho)\,dz \end{aligned} \tag{D.5}$$

where $A(.)$ is the "Albini function" (see Albini, 1985)

$$A(\mu) = \int_{\psi=0}^{\pi/2} \cos\psi \, e^{-\mu(\sec\psi - 1)} \, d\psi \,. \tag{D.6}$$

The Albini function is readily tabulated, and this enables the rapid calculation of $J_i(X)$.

Appendix E
Cold boundary condition

We use the following four asymptotic approximations for large distance X from the flame:

1. The air temperature is approximately ambient, $T_{\text{air}} \approx T_\infty$, and so the convective heat transfer coeficient is approximately constant, equal to $\hbar$, say;

2. For the combustion zone radiation, $J_i(X) \approx 0$;

3. For the radiative cooling of the fuel temperature T, we use the linear approximation

$$T^4 - T_\infty^4 \sim 4T_\infty^3 (T - T_\infty);$$

4. For the flame radiation, if we denote the flame radiation profile with height above the fuel bed by

$$\frac{E_f(z)}{E_{f,0}} = g(z)\,,$$

then, from (C.1),

$$J_f(X) = \frac{2WX}{\pi} \int_{z=0}^{H} \frac{g(z)}{c^2\sqrt{c^2 + W^2}} \, dz$$

where

$$c^2 = (X - z\tan\phi_f)^2 + z^2 \sim X^2 \quad \text{as } X \to \infty.$$

Note that this requires X to be large compared with the flame height H and the bed half-width W. Hence

$$J_f(X) \sim \frac{2W}{\pi X^2} \int_{z=0}^{H} g(z)\, dz = \frac{2WG}{\pi X^2} \quad \text{as } X \to \infty \tag{E.7}$$

say.

Note that for a gaussian flame radiative profile,

$$g(z) = \exp(-(z/\sigma_f)^2), \quad 0 < z < H,$$

we have

$$G = \sqrt{\pi}\sigma_f\{\Phi(\sqrt{2}H) - 0.5\},$$

where $\Phi(\cdot)$ is the gaussian distribution function.

We now use these approximations in the differential equation (23). Letting $\theta = T - T_\infty$ denote the temperature rise, then (23) becomes

$$-R\rho_b c^* \frac{d\theta}{dX} = \alpha\varepsilon_p E_{f,0} \frac{2WX}{\pi} - 4\alpha(\hbar + 4k_r\varepsilon_p\sigma_B T_\infty^3)\,\theta$$

that is,

$$\frac{d\theta}{dX} - a\theta = -\frac{b}{X^2} \tag{E.8}$$

where

$$a = \frac{4\alpha(\hbar + 4k_r\varepsilon_p\sigma_B T_\infty^3)}{R\rho_b c^*} \qquad \text{and} \qquad b = \frac{2\alpha\varepsilon_p E_{f,0} WG}{\pi R\rho_b c^*}. \tag{E.9}$$

Using the boundary condition $\theta = \theta_b$ when $X = X_b$, we can integrate (E.8) to yield

$$\theta_b = be^{aX_b} \int_{X=X_b}^{\infty} \frac{e^{-aX}}{X^2}\, dX = \frac{b}{X_b} - abe^{aX_b} E_1(aX_b), \tag{E.10}$$

where $E_1(.)$ is the exponential integral (see e.g. Abramowitz and Stegun, 1965, eq 5.1.1).

We can solve (E.10) numerically to find X_b for a given θ_b, or we can use the series expansion

$$E_1(x) = \frac{e^{-x}}{x}\left(1 - \frac{1}{X} - \frac{2}{X^2} + \frac{3!}{X^3} + \cdots\right) \quad \text{as } x \to \infty$$

(Abramowitz and Stegun, 1965, eq 5.1.51), which gives

$$\theta_b = \frac{b}{X_b}\left(\frac{1}{aX_b} - \frac{2}{a^2X_b^2} + \frac{3!}{a^3X_b^3} - \cdots\right) \approx \frac{b}{aX_b^2} \quad \text{for large } X \tag{E.11}$$

which we can solve explicitly

$$X_b \approx \sqrt{\frac{b}{a\theta_b}}. \tag{E.12}$$

References

Abramowitz, M. and Stegun, I. A. (1965). *Handbook of mathematical functions.* Dover, New York.

Albini, F. A. (1985). A model for fire spread in wildland fuels by radiation. *Combustion Sci. Tech.* **42**, 229–258.

Albini, F. A. (1986). Wildland fire spread by radiation — a model including fuel cooling by natural convection. *Combustion Sci. Tech.* **45**, 101–113.

Anderson, H. E. (1969). Heat transfer and fire spread. Research Paper INT-69, USDA Forest Service, Intermountain Forest and Range Exptl. Sta., Ogden, UT, USA.

Butler, B. W. (1993). Experimental measurements of radiant fluxes from simulated wildfire flames. In *12th Conference on Fire and Forest Meteorology*, pages 104–111, Bethesda, MD. Society of American Foresters. SAF Publication 94-02.

Catchpole, W. R., Catchpole, E. A., Butler, B. W., Rothermel, R. C., Morris, G. A. and Latham, D. J. (1998). Rate of spread of free-burning fires in woody fuels in a wind tunnel. *Combustion Sci. Tech.* **131**, 1–37.

Cleveland, W. (1985). *The elements of graphing data.* Wadsworth, Monterey, Calif.

de Mestre, N. J., Catchpole, E. A., Anderson, D. H. and Rothermel, R. C. (1989). Uniform propagation of a planar fire front without wind. *Combustion Sci. Tech.* **65**, 231–244.

Dunlap, F. (1912). The specific heat of wood. Technical report, USDA Forest Service. Bulletin 110.

Frandsen, W. H. (1973). Effective heating of fuel ahead of spreading fire. Research Paper 140, USDA Forest Service, Intermountain Forest and Range Experimental Station., Ogden, UT, USA.

Hottel, H. C. and Sarofim, A. F. (1967). *Radiative Transfer.* McGraw-Hill, New York.

Hottel, H. C., Williams, G. C. and Steward, F. R. (1965). Tenth symp. (international) on combustion proc. In *The modeling of fire spread through a fuel bed*, pages 997–1007, Pittsburgh, Pa., USA. The Combustion Inst.

Incropera, F. P. and De Witt, D. P. (1990). *Fundamentals of heat and mass transfer.* Wiley, 3rd edition.

Jarvis, P. G., James, G. B. and Lansberg, J. J. (1976). Coniferous forest. In Monteith, J. L., editor, *Vegetation and the Atmosphere*, volume 2, chapter 7. Academic Press, New York.

McCaffrey, B. J. and Heskestad, G. (1976). A robust bidirectional low-velocity probe for flame and fire application. *Combustion and Flame* **26**, 125–127.

Rothermel, R. C. (1971). An examination of radiation's role in rate of fire spread in wildland fuels. Master's thesis, Colo. State Univ., Ft Collins, Co., USA.

Shaddix, C. R. (1999). Practical aspects of correcting thermocouple measurements for radiation loss. In *33rd National Heat Transfer Conference*, Albuqueque, New Mexico. to appear.

Susott, R. (1982). Characterization of the thermal properties of forest fuels by combustible gas analysis. *For. Sci.* **28**, 404–420.

Thomas, P. H. (1967). Some aspects of the growth and spread of fire in the open. *For.* **40**, 139–164.

Van Wagner, C. E. (1967). Calculations on forest fire spread by flame radiation. Pub., Dept. For. and Rural Develop., Petawawa Forest Experimental Station, Chalk R., Ontario, Canada.

Part 2: State of progress

The pseudo-predictions for coarse excelsior fires are given in Figure 8 of Part 1 of this Final Report of INT-94962-RJVA. These indicate how well ignition temperature can be predicted using the measured variables, such as radiative flux, surface wind velocity and air temperature profile, in the energy balance equation (equation 21 in Part 1). Before prediction of spread rate is possible these measured variables must be modelled, either in terms of reaction intensity or Byram's fireline intensity, or in terms of variables that can be measured prior to the fire – such as packing ratio, fuel depth, moisture content or wind speed. Models in terms of fireline intensity are highly dependent on spread rate, and this may cause convergence problems when solving equation 21, because both sides of the equation tend to be strongly linear in spread rate. Thus, even if a model in terms on intensity fits well, and is physically appealing, we have developed an alternative model in terms of fuel and environmental variables. The submodels considered are given in the next section.

SUBMODELS

Flame height model

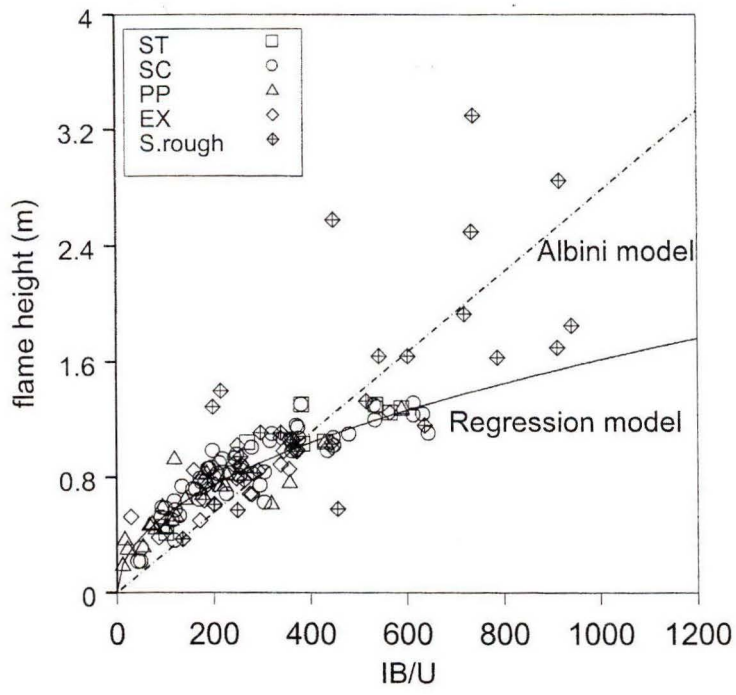

Figure 1. Flame height versus IB/U (wind aided fires)

Albini (1981) gives an approximation to his phenomenological model for flame properties, which predicts flame height h to be proportional to the ratio of Byram's intensity, I_B, to wind speed U. In Figure 1, flame height is plotted against I_B /U. Albini's model (in the form given by Nelson and Adkins (1986)) is overlaid.

It can be seen that the relationship between flame height and the intensity/wind speed ratio is non-linear for our data. It can be modelled as

$$h = 0.0591\ (I_B / U)^{0.4792} \qquad (1)$$

where h is flame height. The regression (on a log scale) has an R^2 value of 0.81.

Nelson (internal report 1996) relates flame height to Byram's intensity alone for field fires in Southern Rough. This implies that the entrainment velocity of air into the flame is proportional to the buoyant velocity, whereas for Albini's model entrainment is assumed to be proportional to wind speed. In Figure 2 flame height is plotted against I_B. Flame height is highly correlated with I_B, but not as strongly as it is with I_B/U. The fitted regression line is

$$h = 0.0601\ (I_B)^{0.4246} \qquad (2)$$

The R^2 value is 0.74. Nelson's fitted line for his field data is shown overlaid.

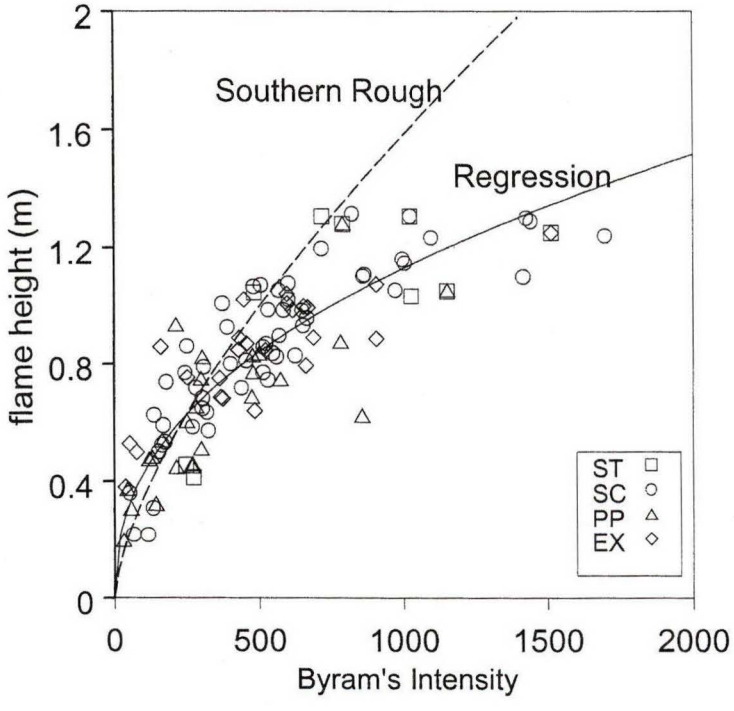

Figure 2. Flame height versus IB (wind aided fires)

Three comments need to be made. Firstly flame height is modelled in terms of Byram's intensity, which is calculated from

$$I_B = H\, w_a\, R$$

where H is the fuel heat content, R is the rate of spread, and w_a is the fuel consumed. The dependence on spread rate means that an extra term in R is added to the energy balance model, and this will change the convergence properties of the equation when solving for R. Flame height is required in the model through the view factor V_F. The

model does not appear to be very sensitive to flame height, and using a submodel dependent on I_B may not be a problem.

Secondly, using I_B as a basis for a submodel requires us to model w_a, or equivalently the efficiency η, where $w_a=\eta w_0$, and w_0 is the fuel loading. A model for I_B is in fact needed in any case for the new fire prediction system. For the flame model w_a should represent the fuel consumed in flaming combustion. Efficiency has been modelled for laboratory data in Catchpole *et al.* (in preparation (a)), but a field model is required. Unpublished data from the European Efaistos project suggest that small pieces of twig within pine needle fuels will cause a significant drop in the combustion efficiency. Modification of Albini and Reinhardt's (1995) BURNUP model may be possible to determine the fuel burned in flaming combustion, and some calibration could be done from the mixed fuel experiments described in Catchpole *et al.* (1993).

Thirdly, it can been seen from Figure 1 that in the Southern Rough the measured flame height was higher than the laboratory flame heights for the same intensity/wind speed ratio. This may be because buoyancy is restricted in the laboratory. It will be necessary to look at data from open tunnels and the field to develop a submodel for flame height that is robust in the field.

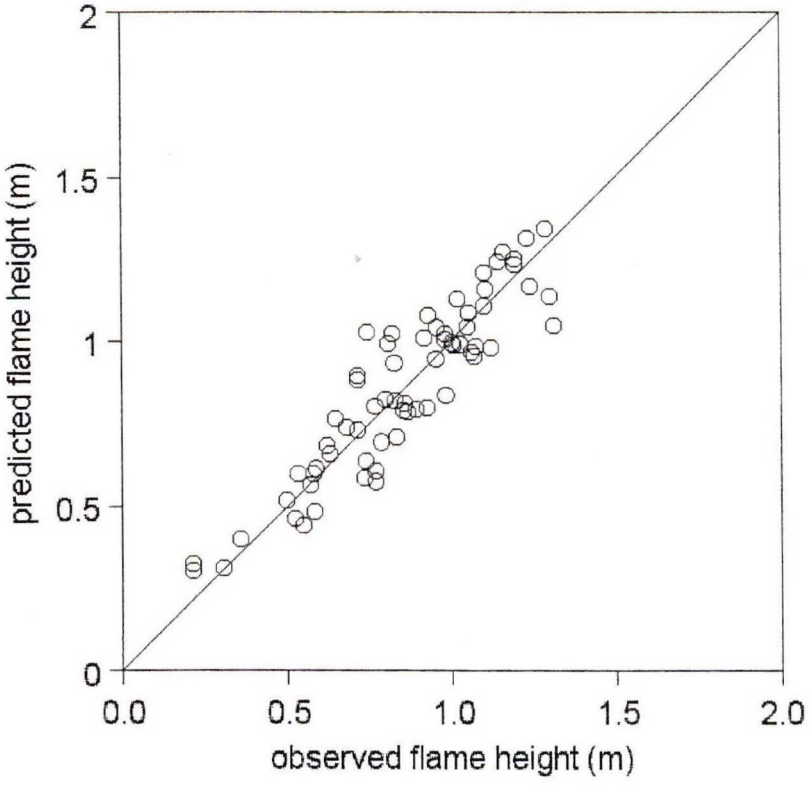

Figure 3. Flame height regression model (coarse excelsior)

Because of possible convergence problems a regression model for flame height in terms of the fuel parameters was developed. The best regression model for *coarse excelsior* (on which most of our modelling was based) was

$$h = 3.2743\ w_0^{\,0.9405}\ U^{0.1129}\ exp(-0.6323\ w_0 - 1.067\ M_f - 17.044\ \beta) \qquad (3)$$

where β, M_f are packing ratio and moisture content, respectively. The R^2 value for the fit is 0.86, and the predicted flame heights are shown plotted against the observed flame heights in Figure 3. The form of this equation includes a damping effect on flame height at high packing ratios and also high loadings. The latter effect is necessary to obtain a good fit, but may be a result of limitations on buoyancy in the tunnel at high fuel loadings. The maximum occurs at a packing ratio of about 0.05 at a fuel depth of 0.075m and at about 0.02 at a fuel depth of 0.15m. With regard to fuel depth, the maximum occurs at a depth of about 0.1m at a packing ratio of 0.03 and at about 0.7m at a packing ratio of 0.005.

Flame angle model

The flame model of Albini (1981) gives an approximate relationship between flame angle and a Froude number based on flame height, Fr(h), of the form

$$tan(\theta) = 1.22\,[\mathrm{Fr}(h)]^{0.5}, \quad \text{where} \quad \mathrm{Fr}(h) = U^2 / (g\,h).$$

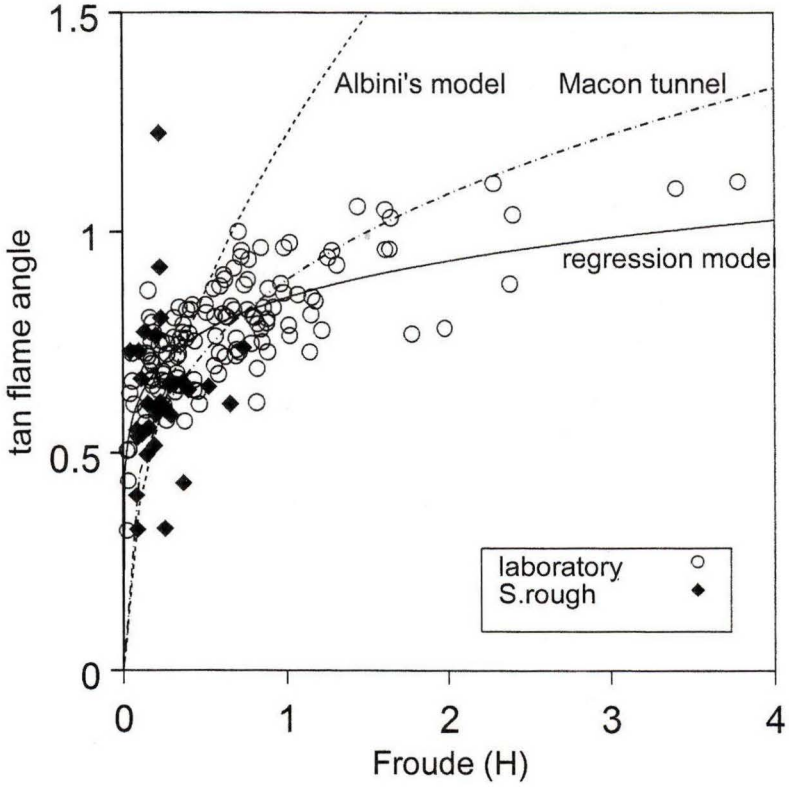

Figure 4. Flame angle versus Froude number in flame height.

A graph of the tangent of the flame angle against the Froude number in flame height is shown in Figure 4. The fitted relationship is much weaker than Albini's, and is given by

$$tan(\theta) = 0.851[\mathrm{Fr}(h)]^{0.1356} \qquad (4)$$

This has an R^2 value of 0.54. Nelson and Adkins (1986) burned *Pinus eliottii* needles in the USFS wind tunnel in Macon, GA. The tunnel is closed, with slightly smaller dimensions than the tunnel at the Fire Science Laboratory in Missoula. The relationship obtained by Nelson and Adkins is closer to the relationship obtained in Missoula, but somewhat stronger, and is shown in Figure 4 together with Albini's model.

Other predictor variables, such as the Froude number based on flame depth, and the ratio of the 'power of the wind' to the 'power of the fire' (Byram 1959) can be used. These are discussed in Catchpole *et al.* (in preparation (b)), where it was concluded that these other relationships yield very similar results.

The same comments given in the section on flame height apply to flame angle. In particular data from open tunnels and the field are essential. It must be noted that field data on flame angle is very scarce. Flame angles from Southern Rough fires, measured by video analysis (McMahon *et al.* 1986) are shown in Figure 4.

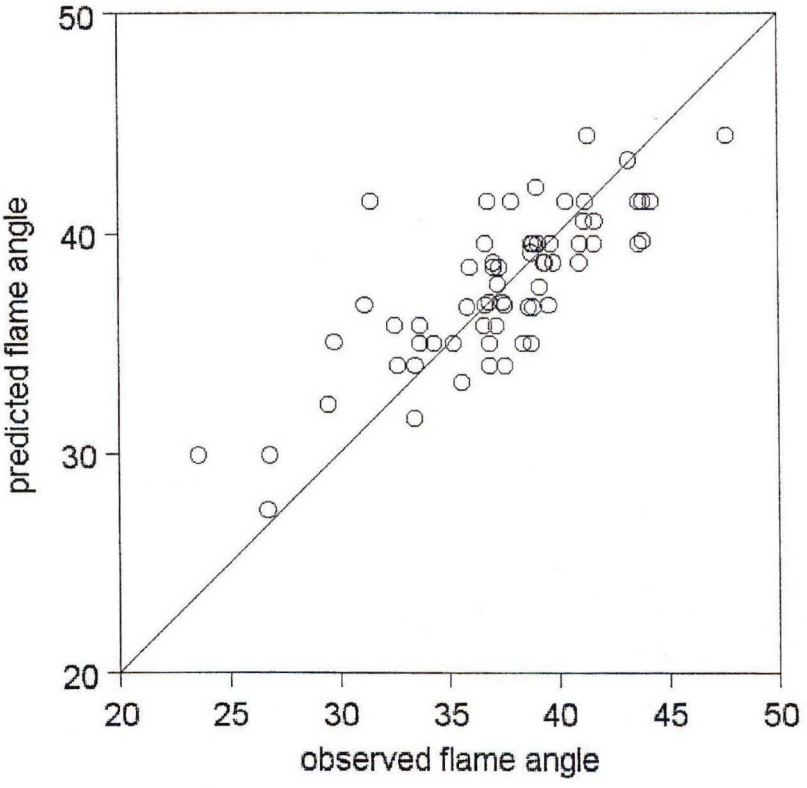

Figure 5. Flame angle regression model (coarse excelsior)

Flame emissive flux: (a) Qmax

From the fits of the Gaussian radiation model to the emissive flux data (from the bolometers at different heights) a value of the base radiation, *Qmax*, and the

standard deviation σ_G was obtained for each set of fires. *Qmax* is strongly related to Byram's intensity, as shown in Figure 6. The regression curve is given by

$$Qmax = 0.5869\ I_B^{\ 0.7408} \qquad (6)$$

The R^2 value for the logarithmic fit is 0.56. The problem with this model is that it is highly dependent on spread rate through I_B, which we know causes convergence problems. Ideally a physically-based model for *Qmax* is required, and work on this is in progress.

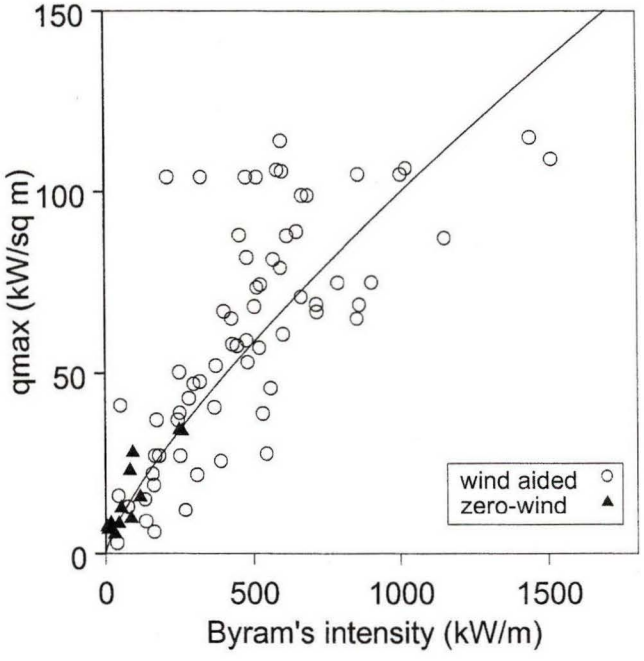

Figure 6. Flame base radiative flux (Qmax) in terms of Byram's intensity

In the meantime we require some interim model for *Qmax* that will enable us to solve the energy balance equation and predict spread rate. A possible interim model is the regression model for *coarse excelsior* shown in Figure 7. The model is given by

$$Qmax = 4338\ \beta^{0.7185}\ \delta^{0.4359}\ U^{0.6936}\ exp(-4.221\ M_f - 19.817\ \beta) \qquad (7)$$

where δ is the fuel bed depth. This has an R^2 value of 0.52. The behaviour of *Qmax* at high packing ratios is to be investigated with experiments described in the study plan. For this interim model the maximum of *Qmax* as packing ratio increases occurs at a packing ratio of about 0.035.

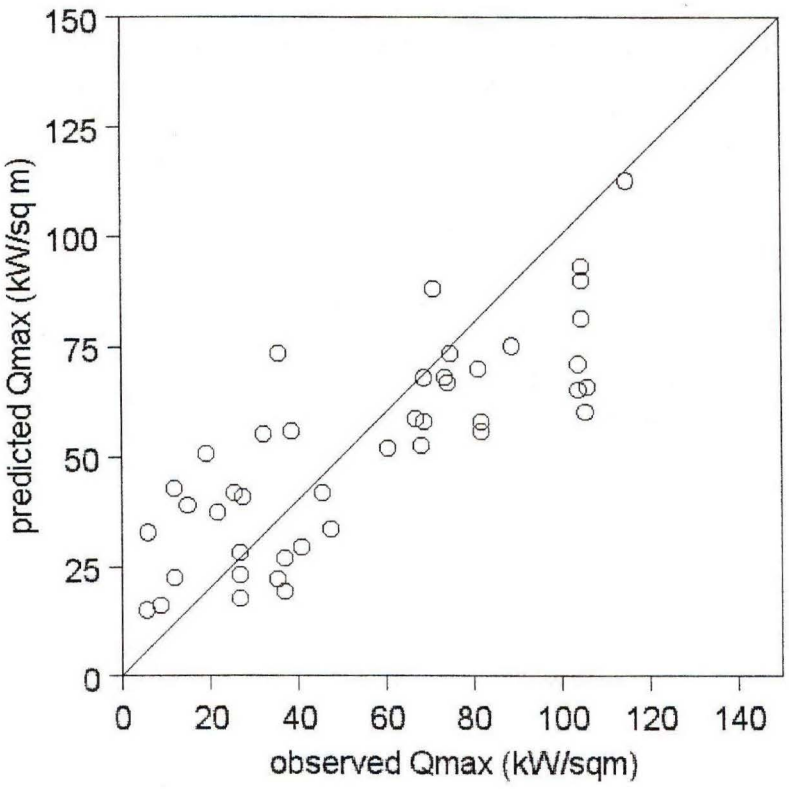

Figure 7. Flame base radiative flux (Qmax) regression model (coarse excelsior)

Flame emissive flux: (b) σ_G

The parameter σ_G describes how emissive flux decreases with the ratio of height above the fuel to flame height. For the data sets for which we had estimates of σ_G, we could find no relationship with fuel or environmental parameters, except for a slight, non-significant, decrease with moisture content. An average value of 0.36 can be used for modelling. Emissivity has been related to flame depth, and since the ratio of flame length to flame depth is fairly constant in the laboratory fires, this is consistent with σ_G being constant. An attempt to refit the Gaussian curves using this average value of σ_G is being made, to see whether this decreases the variability in *Qmax*.

Combustion zone angle

Using a camera close to the combustion zone, side views of the fires show that in light packing ratio fires the angle of the combustion zone is close to the flame angle. This then, is the assumption made in the model. In fires in fuels with heavier packing ratios the combustion zone angle may be less than the flame angle, so the assumption would cause under predictions of combustions zone radiation. However in such fires the attenuation of combustion zone radiation will be high, and the combustion zone radiation small compared to the flame radiation.

Combustion zone emissive flux

The combustion zone emissive flux, Qc, is weakly related to Byram's intensity (see Figure 8). A model for Qc in terms of Byram's intensity is

$$Qc = 10.30\, I_B^{\,0.346} \qquad (8)$$

The regression has an R^2 value of 0.40. Since it is preferable to avoid using Byram's intensity as a predictor variable (because of its strong relationship to spread rate) and as the R^2 value for equation (8) is low, it seems reasonable to model the emissive power as a constant. $Qc = 100$ kW/m^2 is used as a submodel. This will overpredict badly for fires with intensity less than 200-300 kW/m, so a possible alternative would be to use $Qc = 50$ kW/m^2 below an intensity of 250 kW/m.

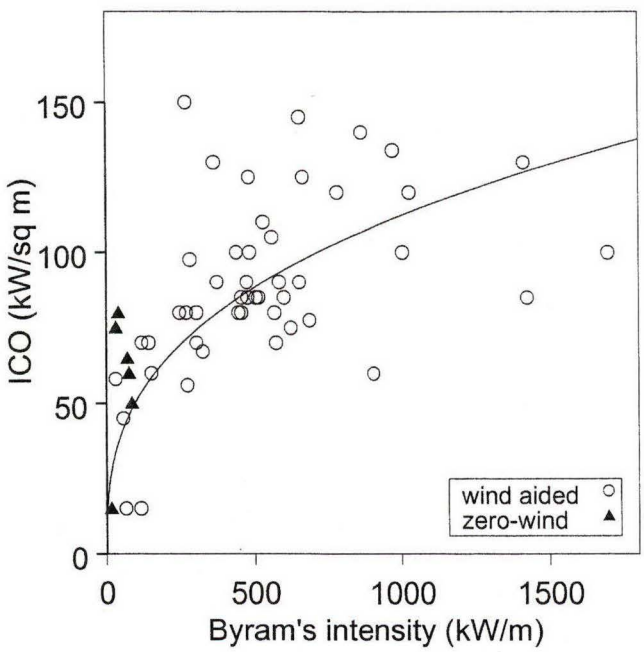

Figure 8. Combustion zone radiative flux (Qc) in terms of Byram's intensity

Surface velocity: (a) far from flame

A division is made between the region far from the flame where the air flow tends to cool the fuel particle, and the region of heating near the flame. From inspection of temperature profiles the criterion for the division was taken as the point at which the air temperature first rises more that 50 degrees above the fuel temperature. This tends to happen with a sudden burst of heating (see Figure 9). The keil probe readings from fire ignition to this cut-off point are averaged. These averages can be shown to increase with wind speed.

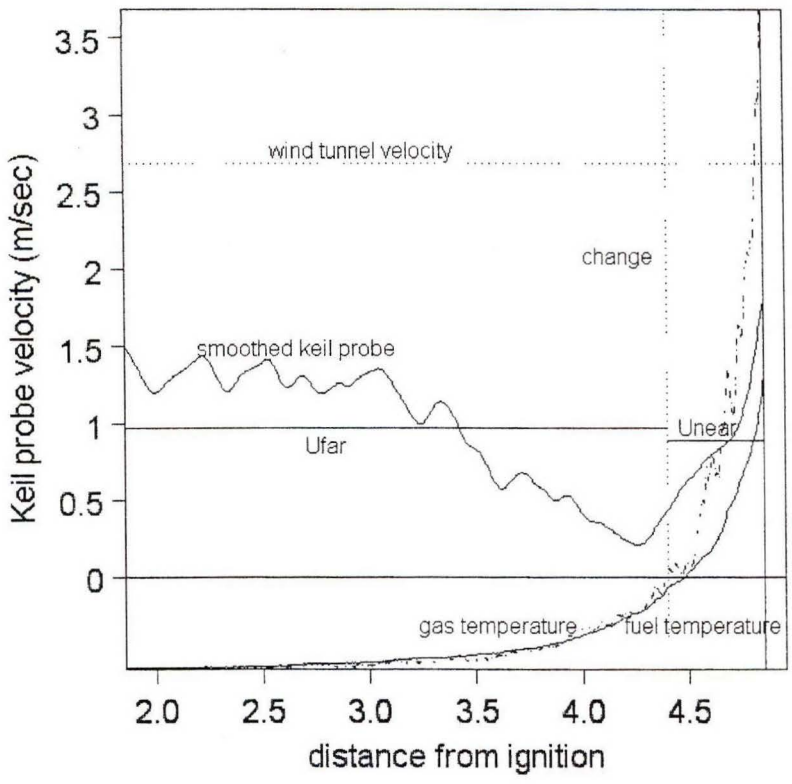

Figure 9. Surface velocity and thermocouple profiles

They are also weakly correlated with $s\beta$, the surface area of fuel, per volume of fuel bed, and with $s\beta\delta$, the surface area of fuel per surface area of fuel bed. A possible model for the far surface velocity *Ufar* is given below

$$Ufar = 0.8\ U\ exp\ (-s\beta/100) \qquad (9)$$

The predictions using Model (9) are shown in Figure 10 for sticks and excelsior (the fit to pine needle fires is poor). The R^2 value is only 0.36 for the coarse excelsior fires. The model is not suitable for zero-wind fires where there is an inflow towards the flame. A series of experiments have been designed to produce a better model by comparing velocities from hot film anemometers with keil probe estimates of velocity in and above the fuel bed in the absence of fire.

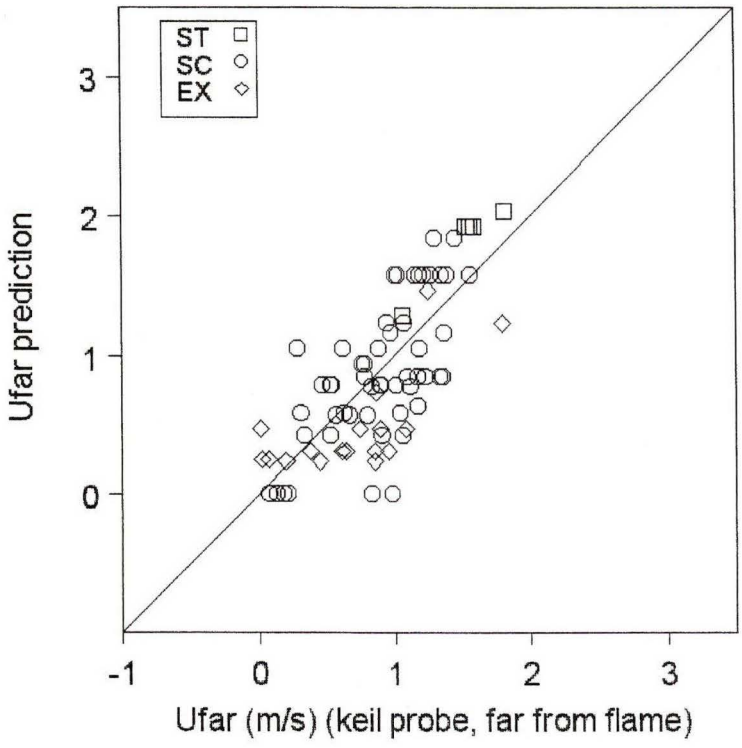

Figure 10. Model for Ufar (surface velocity far from the flame interface)

Surface velocity: (b) near the flame

In the region, close to the flame, the velocity drops, and in low wind-speed fires may reverse in direction. Closer to the flame the keil probe trace rises rapidly, and may reach ambient tunnel conditions. We have doubts about the ability of the keil probe to measure velocities accurately in this region of rapidly changing temperature, where corrections for changes in air density (which assume steady-state conditions) may not be valid. The mean velocities in this region are very variable. Like the far velocity regions they show some relationship with wind speed and fuel properties.

The acceptance angle for the keil probe is high (30°), and it seems likely that the *Unear* average velocities include the effect of buoyancy near the fire. Several different formulations for the buoyant velocity in the flame were tried (see Nelson 1996), but none yielded any correlation with *Unear*. Nevertheless a model was formulated including the effect of buoyant velocity in the form

$$Unear = (W_b^2 + 0.6*U^2)^{0.5}\ exp(-s\beta/100) \qquad (10)$$

where W_b is the buoyant velocity on the fuel surface. W_b can be calculated from the reaction time and the spread rate (see Nelson 1996). Its dependence on spread rate could lead to convergence problems. As it is reasonably constant compared to wind speed an average value of 1 m/sec has been used for modelling. This could be modified by a reduction at higher moisture contents and higher loadings. Model (10)

is shown in Figure 11 for the stick and excelsior fires. Again, the correlation is very poor.

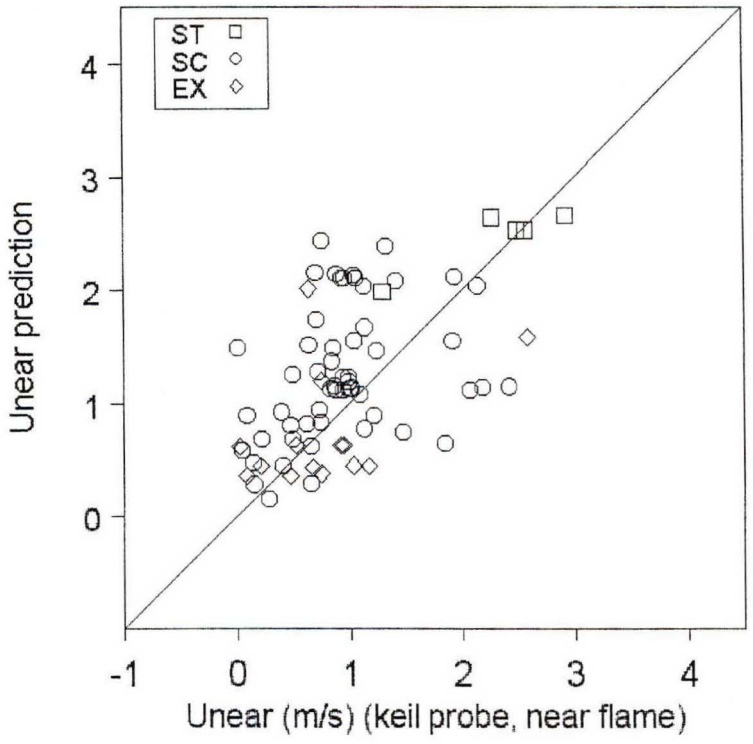

Figure 11. Model for Unear (surface velocity near to the flame interface)

Investigation of the goodness of fit of the temperature-time curves near the flame interface (to be described later) showed that the prediction of ignition temperature was sensitive to the form of the relationship between the surface velocity near the flame and the fuel parameters s and β. The surface area of the fuel per volume of fuel bed (given by $s\beta$) constitutes a drag effect on the velocity. Further models need to be developed and validated after more investigation of the drag effects through the fuel bed are investigated.

It may be better to model the surface velocity in more detail, incorporating explicitly the reduction in velocity close to the flame. Inflows from the sides of the fire may have an important effect, and their magnitude should be investigated.

Gas temperature

The gas temperature profile ahead of the ignition interface is modelled as an increasing exponential with maximum at the interface. The form of the model used is

$$T_a = T_{amb} + (T_{max} - T_{amb}) \exp(\lambda_t (t - t_{ig})) \qquad (11)$$

Here T_a is the temperature of the gas ahead of the interface, T_{amb} is the ambient temperature of the surroundings, T_{max} is the air temperature at the time of ignition of the fuel particle, t is time, t_{ig} is the ignition time of the fuel particle, and λ_t is the

constant describing the rate of increase of gas temperature with time. The reciprocal of λ_t may be thought of as the characteristic heating time in front of the flame interface. This form of temperature model was fitted to the corrected gas temperature for every set of fires, and the best estimates of T_{max} and λ_t were found. An example of equation (11) fitted to a gas temperature profile is shown in Figure12.

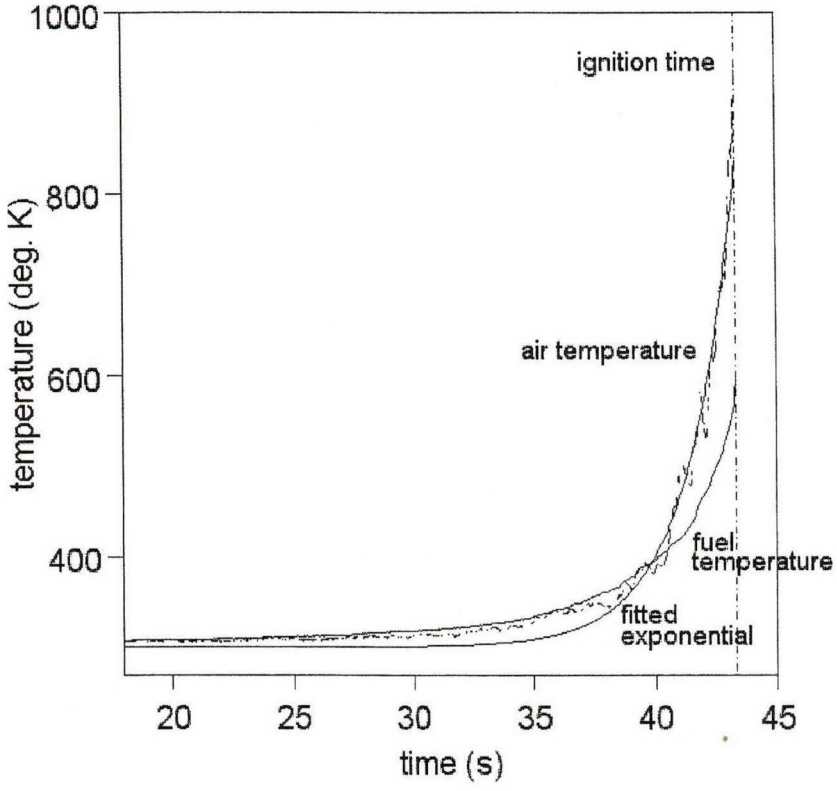

Figure 12. Surface and corrected thermocouple profiles, and exponential curve fitted to the corrected air temperature.

Models for T_{max} and λ_t are required. The maximum temperature, T_{max}, decreased slightly (but non-significantly) with moisture content, but the R^2 value was only 0.08. It did not appear to be related to any other fuel or environmental variables, so an average value of 885°K is used for T_{max}.

Since the temperature ahead of the fire should not change as rate of spread is varied in the convergence process, a model for the decay rate λ_d of gas temperature with distance ahead of the fire (rather than time) is used in the convergence program, and λ_t is then obtained from $\lambda_t = R\,\lambda_d$. Thus as R is varied the gas temperature decay with distance in front of the fire is fixed. λ_d was obtained from λ_t for the set of coarse excelsior fires with measured *Qmax* and keil probe velocities, and a regression model was developed to predict λ_d. The best fitting model was

$$\lambda_d = 10.518\ U^{-0.7697}\ W_0^{\ 0.1416} \qquad (12)$$

The R^2 value for the fit is 0.85. The predicted values of λ_d are shown plotted against the values of λ_d obtained from curve fitting in Figure 13.

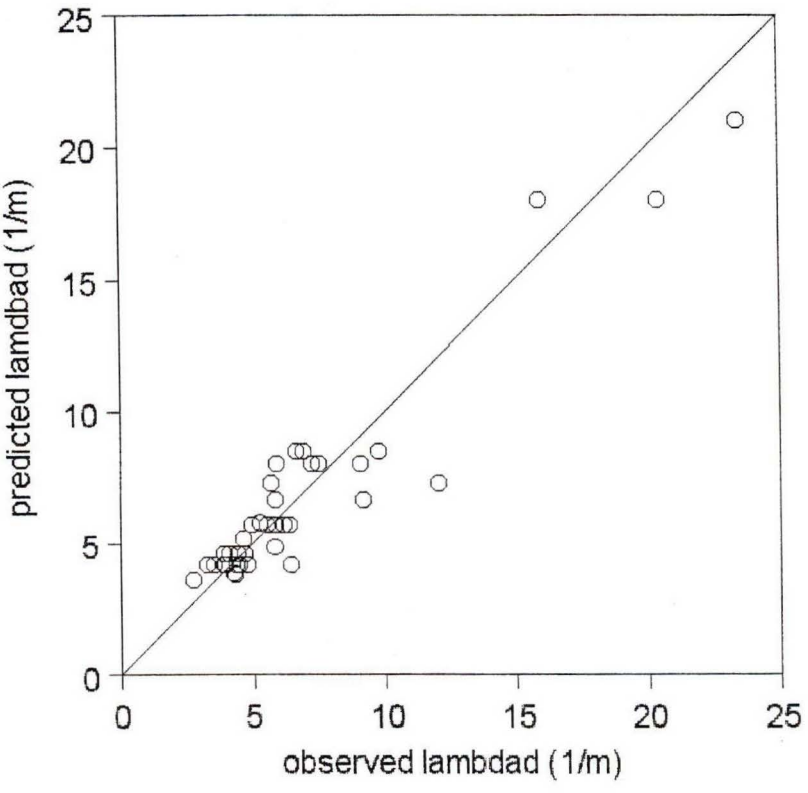

Figure 13. Regression model for λ_d (coarse excelsior)

Change from ' far' to 'near'

The surface velocity profile ahead of the flame interface is modelled as a step function equal to *Ufar* before the change and *Unear* after the change. This model is shown overlaid on the surface velocity profile from one of the fire sets in Figure 9. The change from cooling to strong heating occurs in Figure 9 about $2/\lambda_d$ meters from ignition. Examination of several keil probe traces and the corresponding gas velocity traces showed that this seemed a reasonable estimate for the position of the change.

It should be noted that this step function gives a poor fit to the velocity traces, but it may not be worth modelling the wind profile more accurately, as the step submodel gives very similar predictions of the fuel temperature to those obtained using the velocity profiles from the keil probe. The model seems fairly insensitive to the 'far' surface wind speed. The 'near' surface wind speed is very much a matter of conjecture as the keil probe can give readings higher than the ambient tunnel wind speed, and may be totally misleading in this region. A model based on the effect of the drag on the buoyancy may well be better than a model based on the keil probe.

Predicting fuel temperature using the submodels

To predict spread rate it is important to get a good estimate of the fuel temperature at the time of ignition. Thus our criterion for goodness of fit for the fuel temperature was that it predicted ignition temperature well. However if the physical

model is correct it must also give good predictions of fuel temperature over the whole temperature profile. Models that fitted well were always checked as to how well they predicted the whole range of fuel temperatures.

In the following sections the submodels used were ones that depended only on the fuel and environmental parameters, and not on spread rate. In the next stage of the program we will check how the dependence of the submodels on spread rate will affect convergence.

The best fit to fuel temperature was found with submodels in Table 1:

Table 1.

flame height	equation (3)
flame angle	equation (5)
Qmax	equation (7)
σ_G	0.36
Qc	50 kW/m^2, I_B <250 100 kW/m^2, I_B>=250
Ufar	equation (9)
Unear	equation (10)
T_{max}	885°K
λ_d	equation (12)
change	2/ λ_d

The pseudo-predicted values of spread rate for coarse excelsior are plotted against the observed value in Figure 14. The pseudo-predicted values of spread rate R_p are given by

$$R_p = R*(Tp[n]-Tamb)/(Tig-Tamb) \qquad (13)$$

where R is the observed spread rate, *Tp[n]* is the predicted fuel temperature at the time when the observed fuel temperature is at ignition, *Tamb* is ambient temperature and *Tig* is ignition temperature.

The fit is good for the fires for which *Qmax* was measured, and on which the gas temperature profile model (12) was based (shown as open circles in Figure 14), but the fires not previously included, which had higher packing ratios, overall, tend to be overpredicted. The overall fit of the model had mean absolute error (MAE) equal to 0.0097 m/s. The more recent fires were at a higher packing ratio, on average, and appears that there is an effect of packing ratio that has not been modelled. The convection near the interface is critical in determining the fuel temperature at ignition. All the submodels in Table 1 (except the model for 'change') were used to obtain the corrected air temperature, and equation (11) was refitted. Another model for λ_d was then formulated. In this model the load effect was less than in (11), and this would not did help the overpredictions.

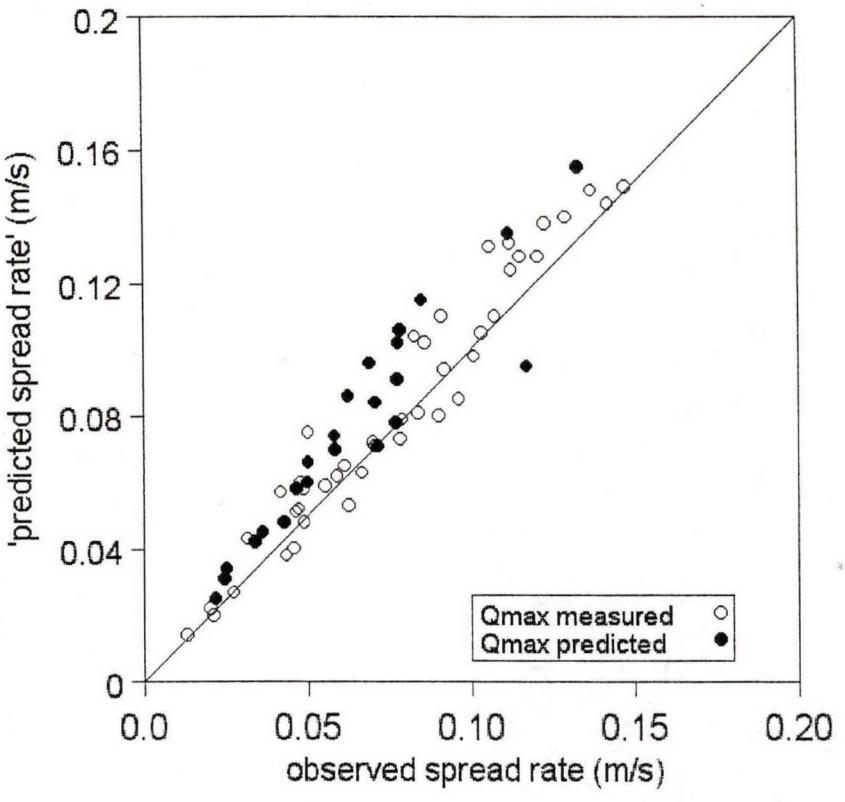

Figure 14. Pseudo-predictions from submodels in Table 1.

The submodel for *Unear* in equation (10) was then modified to

$$Unear = 2.5\ sqrt\ (1+0.6*U^2)\ exp(-s\beta/15) \qquad (14)$$

This gave a much lower *Unear* at higher packing ratios, and a better fit to ignition temperature was obtained, as shown in Figure 15. The MAE in this case was 0.0091 m/s, and the bias due to packing ratio was decreased considerably. The submodel (14) is heuristic, and needs verification.

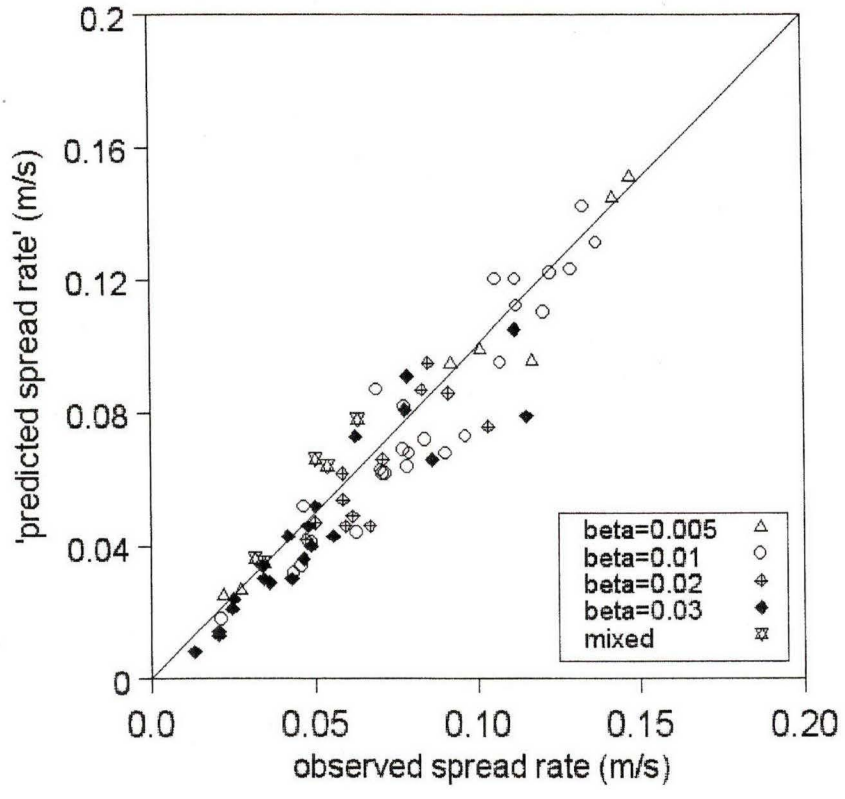

Figure 15. Pseudo-predictions using modified submodel for Unear in (14)

Predicting rate of spread

Predictions of spread rate are obtained by solving the differential equation (equation (21) in Part I of this final report), and finding the spread rate that reduces the absolute value of the difference between ignition temperature and predicted ignition temperature. The predicted values of spread rate for coarse excelsior using the models in Table 1 (with equation 10 replaced by equation 14) are plotted against the observed value in Figure 16.

It can be seen that this gives a much worse fit than Figure 15 (MAE =0.015 m/s). However, it is difficult to do much better than the predictions shown in Figure 15 predict the ignition temperature (when using submodels of flame height, radiation etc.), and so one cannot hope to do much better than the predictions in Figure 16 predict spread rate using this approach. The empirical model, given in Catchpole *et al.* (1998b), is shown fitted to the same coarse excelsior fires in Figure 17 for comparison. Here the MAE = 0.010 m/s. This is obviously an improvement, but the physical model has some advantages, which will be discussed later.

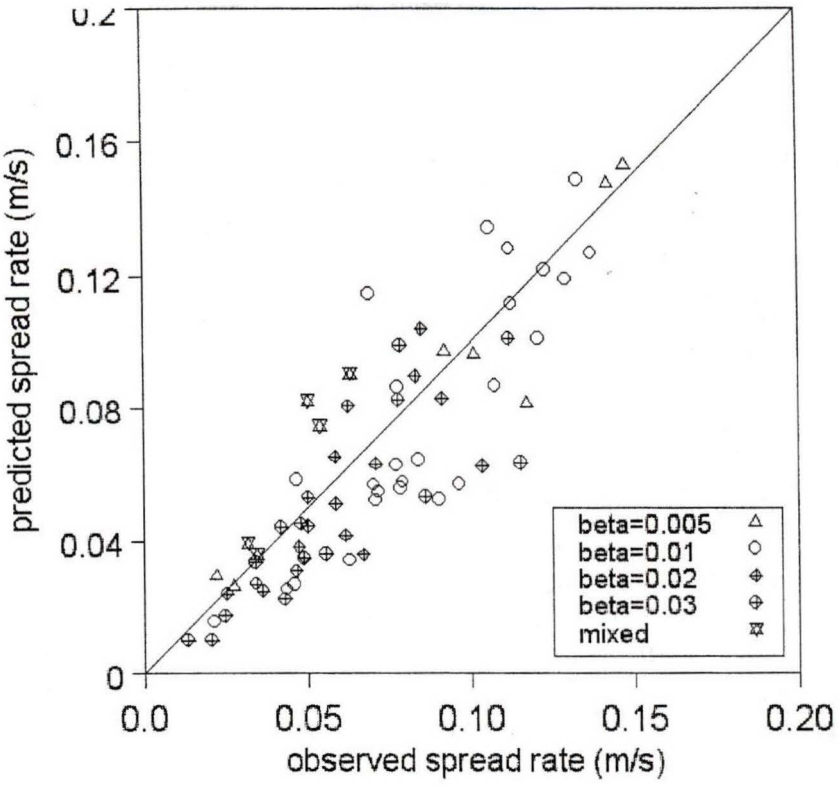

Figure 16. Predicted spread rates using modified submodel for Unear in (14)

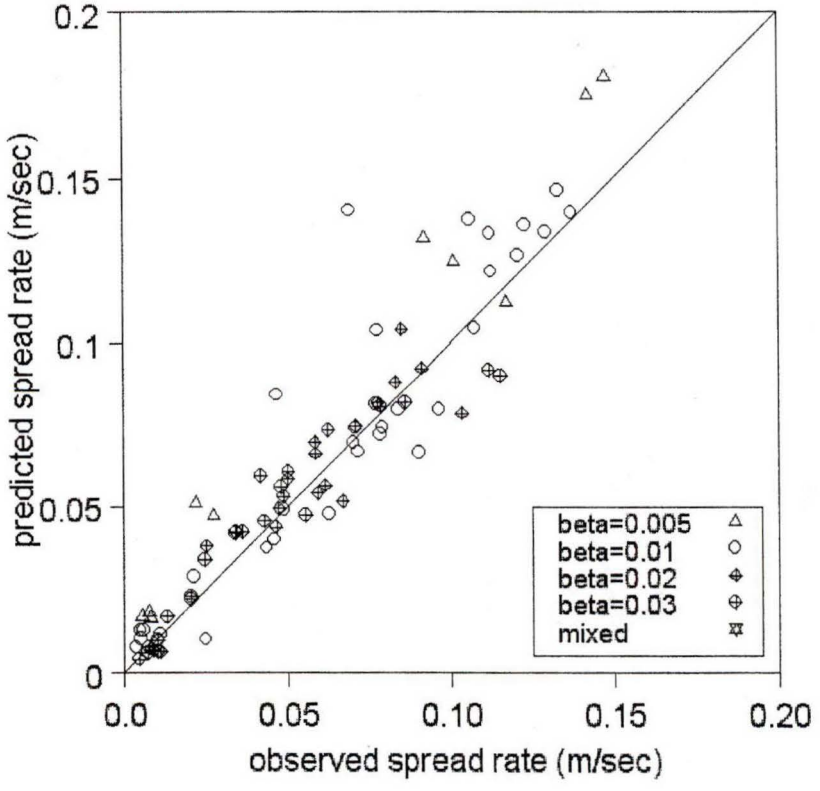

Figure 17. Predicted spread rate using the empirical model of Catchpole *et al.* (1998)

SENSITIVITY AND BEHAVIOUR OF THE MODEL WITH FUEL AND ENVIRONMENTAL CONDITIONS

In this section the behaviour of the spread rate predictions as the fuel and environmental parameters vary is considered. Predictions are matched against data from Missoula and in some cases, other laboratory data.

Packing ratio

Conditions were set at U= 1.8 m/s, δ = 0.076 m, M_f= 0.05, and packing ratio was varied between 0.005 and 0.05. Using equation (14) did not give enough damping effect of packing ratio at higher packing ratios. The empirical model, shown overlaid on Figure 18, has a similar fault. The effect of packing ratio depends heavily on the drag effect on *Unear*. It will be necessary to look again at the effect of packing ratio when more information is known about the effect of drag in the fuel bed and the effect of packing ratio on the flame emissive power for higher packing ratios.

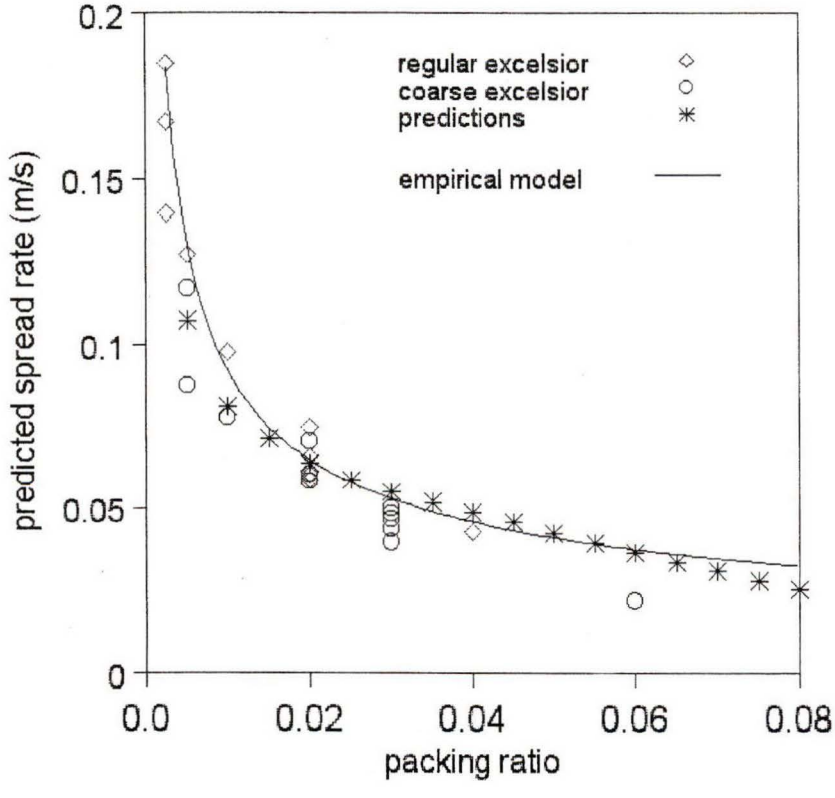

Figure 18. Predicted effect of packing ratio on spread rate.

Wind speed

Conditions were set at δ = 0.076 m, M_f = 0.05, β=0.005 and β=0.02. Wind speed was varied between 0.5 and 5 m/sec. The relationship between spread rate and wind speed was slightly greater than linear, as seen in Figure 19, and corresponded quite closely to the relationship in the experimental data. The empirical model has a

slightly less than linear relationship. The predictions for the β=0.02 fires at wind speeds of greater than 3 m/sec deviate considerably from the empirical model predictions.

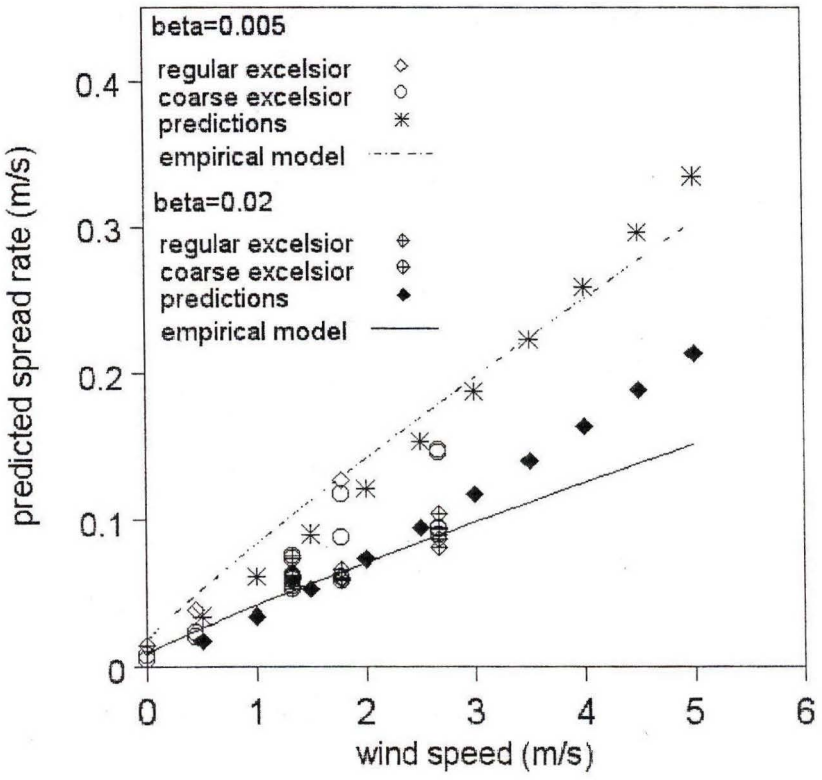

Figure 19. Predicted effect of wind speed on spread rate.

Moisture content

Conditions were set at U = 1.8 m/s, δ = 0.076 m, β=0.005 and β=0.02. Moisture content was varied between 0.025 and 0.25. The predicted values were close to the observed values (see Figure 20), although both the physical model and empirical model may be overestimating the moisture damping at low packing ratio. At present the spread rate model only gives good predictions for coarse excelsior. It has been shown (Wilson 1990, Catchpole *et al.* 1998b) that the decrease in spread rate with increasing moisture content depends on surface area to volume ratio, as well as on packing ratio (possibly a dependence on σβ). This damping effect can be seen to be reflected in the decrease in flame length with increasing moisture content (see draft flame paper). It may be possibly to model moisture damping at other surface area to volume ratios than that of coarse excelsior, and at low packing ratios, through the damping effect on the flame length. On the other hand, the model is not very sensitive to flame length. It will therefore probably be necessary to model this effect using a modified model for the radiative emissive power.

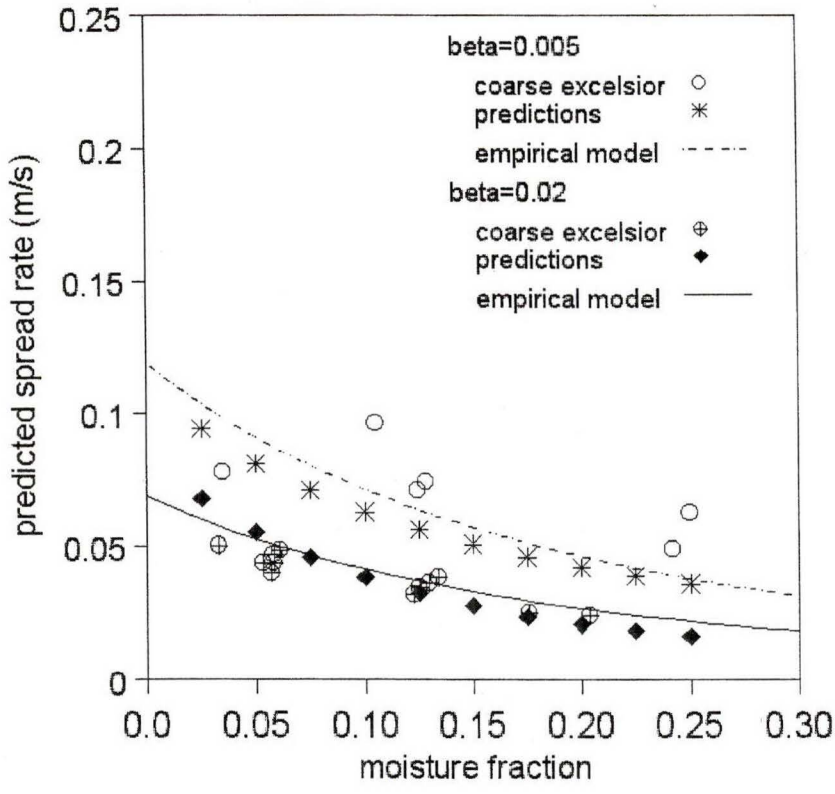

Figure 20. Predicted effect of moisture content on spread rate.

Fuel bed depth

Conditions were set at U = 1.8 m/s, M_f = 0.05, β = 0.005 and β = 0.02. Fuel bed depth was varied between 0.03 and 0.3 m. The experimental data show no consistent effect of fuel bed depth. The model predicts virtually no effect of depth for the lower packing ratio, and an increase with fuel bed depth for the higher packing ratio (see Figure 21). While this is not reflected in the experimental data, it makes sense that for heavier loads flame radiation is more important than at lighter loads, and the spread rate increases with fuel bed depth because of the increased radiative transfer. The depth effect in the laboratory may be suppressed by restrictions on buoyancy and fuel bed width. However the depth effect is probably reflected in field experimental results. Cheney *et al.* (1993) found that fuel depth had no effect in grassfires (where the loading averages 0.35 kg/m^2), but Catchpole *et al.* (1998a) found that spread rate was proportional to the square root of fuel bed depth in shrubland fuels, where the fine fuel loading averages about 2 kg/m^2.

The empirical model has no effect of fuel bed depth. It overpredicts for the coarse excelsior fires where β=0.005. The model was developed before these experiments were performed.

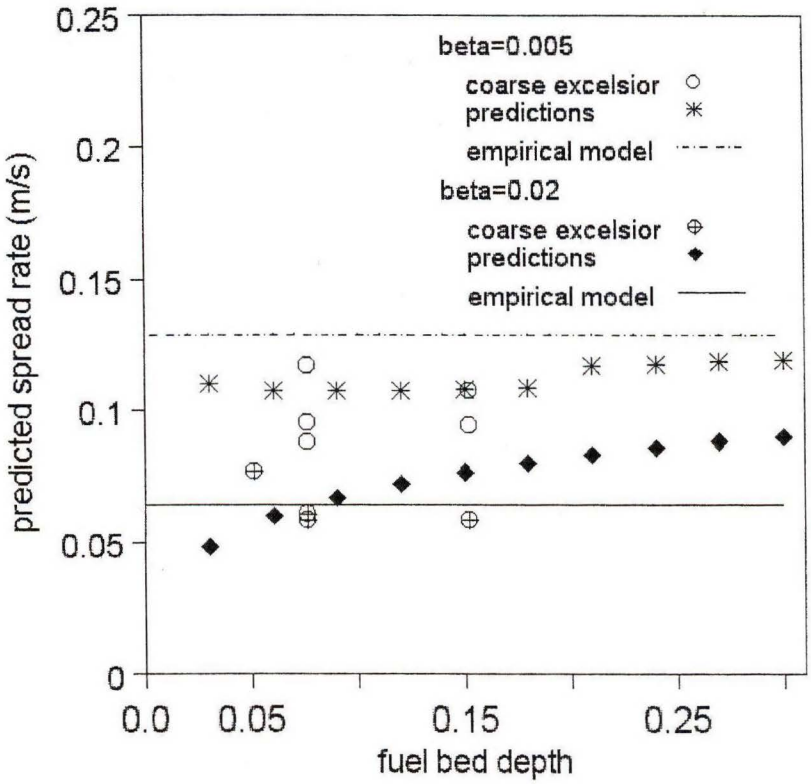

Figure 21. Predicted effect of fuel bed depth on spread rate.

Surface area to volume ratio

For reasons that we do not understand, our model overpredicts badly for fuels with surface area to volume ratio greater than that of coarse excelsior (about $3100m^{-1}$). As can be seen from equation 21 in Part 1 of this Final Report the heat transfer rate should be highly dependent on surface area to volume ratio. The only moderating effects are the drag effect modelled through *Unear* and *Ufar*, and any effect that may be built into the other submodels. Catchpole *et al.* (1998b) showed experimentally that at a packing ratio of 0.02 the propagating flux (the right-hand side of equation 21 in Part 1) was independent of surface area to volume ratio. For the fires reported as the comparative experiments in Catchpole *et al.* (1998b) the flame height, flame angle and *Qmax* are also similar. It would seem that only the drag effect can be moderating the surface area to volume effect in the model.

On the other hand, at a packing ratio of 0.005 spread rate in regular excelsior is about 1.5 times that in coarse excelsior (see Figure 22). Predictions from the model for the conditions in Figure 22 (U = 1.8 m/s, M_f = 0.05, δ = 0.075 m) are shown in the Figure. Until (and if ever) we understand the reasons for the overpredictions it will be necessary either to use some intermediate value of surface area to volume ratio, somewhat higher than $3100m^{-1}$ for low packing ratio fires, or to adjust the predicted spread rates to agree with the experimental data.

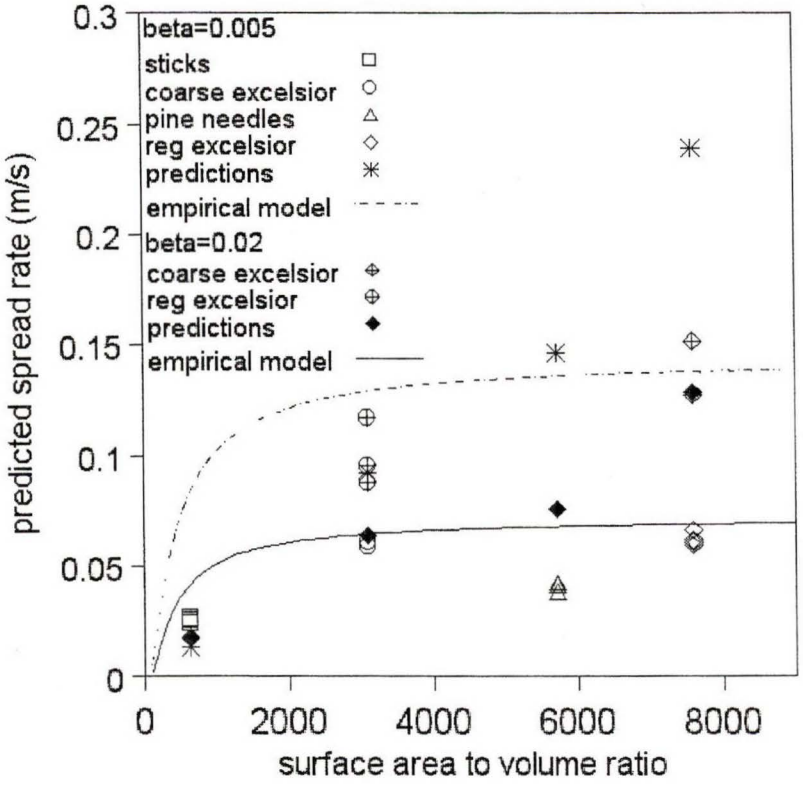

Figure 22. Predicted effect of surface area to volume ratio on spread rate.

Slope

Radiative heat transfer ahead of the fire is increased on a slope because the flame angle and flame height both increase. The increase of radiative transfer with slope angle has been modelled by Pagni and Peterson (1973). Rothermel (1972) reports the effect of slope on spread rate for zero-wind fires in terms of packing ratio and slope angle. More recently, experiments on slopes in zero-wind, done in the framework of the EU project EFAISTOS, was reported by Dupuy (1995). Spread rate for fires on slopes is also reported in Weise and Biging (1997) who used a small wind tunnel with a sloping floor.

To predict spread rate for zero-wind fires on slopes we used a linear increase in flame height to 1.5 of the flame height at zero slope when the slope angle was 30°, based on unpublished data from from INRA (France), produced during the EU funded EFAISTIOS project. Slope had a much greater effect on flame height in the Weise and Biging (1997) experiments, but sensitivity analysis showed that the predictions on a slope were not very sensitive to flame height. Flame angle was assumed to be equal to the slope angle. We used a wind speed of 0.05 m/sec, as the model has not been extended completely to zero-wind fires.

Figure 23 shows spread rate versus slope for zero-wind fires in *Pinus pinaster*, surface area to volume ratio about 4400 m^{-1}, and packing ratio 0.02. The predictions are overlaid. There were convergence problems at low slopes, but the predictions seem reasonable at higher slopes. Figure 23 also shows the zero-wind stick data from

Weise and Biging (1997) (surface area to volume ratio 2275 m^{-1}, and packing ratio 0.008). Predictions are overlaid. These underestimate the slope effect at the higher slope.

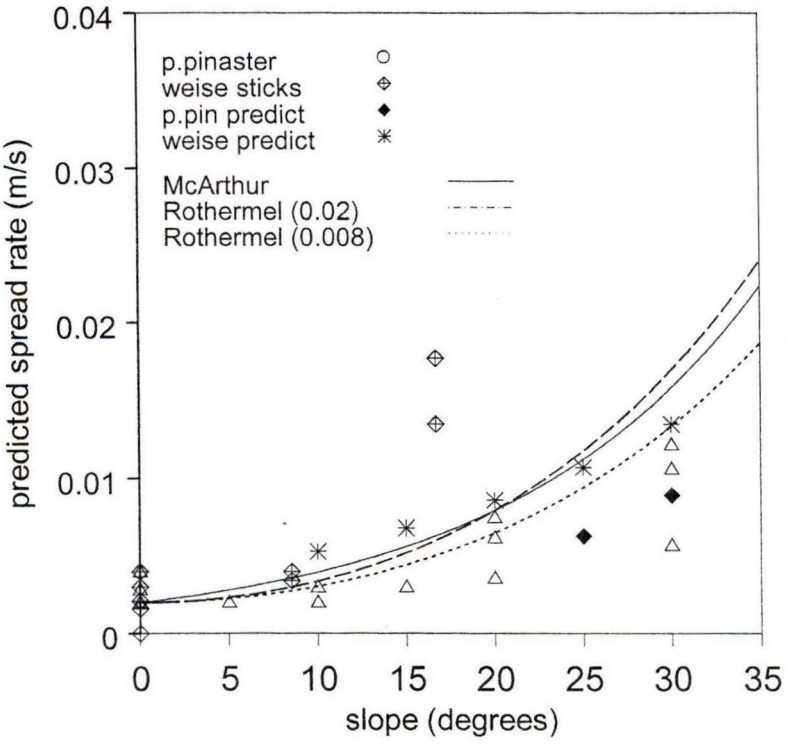

Figure 23. Predicted effect of slope on spread rate in zero-wind fires

Predictions from the slope effects from the Rothermel model and the Australian McArthur Forest meter are also shown. These both overestimate the slope effect in the *Pinus pinaster* data, and underestimate the slope effect in the Weise and Biging data.

If necessary an additional slope effect may be given by increasing the convectional heat transfer. This may be done by increasing the heat transfer coefficient, increasing the gas velocity, and/or increasing the distance ahead of the flame interface where the gas temperature begins to rise dramatically. There seems no reason to increase the heat transfer coefficient. An idea of the increase in gas velocities with slope may be obtained from wind profile studies reported by Ventura and Mendes-Lopes (pers. com. on file at ADFA). For information on temperature profiles in fires on slopes we have information from the experiments conducted by Weise. In these experimental fires pairs of thermocouples in the fuel and an adjacent air thermocouple were used. Preliminary analysis of this data showed that the fuel temperatures were poorly predicted with the model described above. There is a question as to how the depth that the thermocouples were buried in the sticks may affect their temperature response. However it may be possible, with some adjustments to the constants in the model, to use the data to determine how slope affects the air temperature profile ahead of the fire.

If necessary the submodel for λ_d in equation (18) could be modified using

$$\lambda_d = \lambda_{d0} \exp(- k\theta) \quad (15)$$

where θ is the slope angle, λ_{d0} is the value of λ_d with a slope of 0°, and k is some fitted constant.

Spread rate for fires in wind and slope has been reported by Weise and Biging (1997) and Mendes-Lopes *et al.* (1998). The physical model (with no modification, except for the flame angle being set equal to the slope angle) was used to predict spread rate for fires on positive slopes at windspeeds of 1 m/sec for these data sets in Figure 24. Backing fires and negative slopes will be considered later. The model overpredicts spread rate for the Weise and Biging fires, where the effect of slope appears to be moderated by the effect of wind. The physical model behaves more like the multiplicative McArthur slope model. The model overpredicts badly for the *P. Pinaster* fires reported by and Mendes-Lopes *et al.* (1998). A submodel for the flame angle on a slope is needed, possibly in terms of the Froude number.

There is a question of quality of data for these wind-aided fires on slopes in small laboratories where the boundary layer probably is far from realistic. Data may soon be available from the EU project INFLAME where fires were burned on slopes in shrubland which had ignition lines of about 50m (Viegas 1999). These may help to resolve the question of the combined effect of wind and slope.

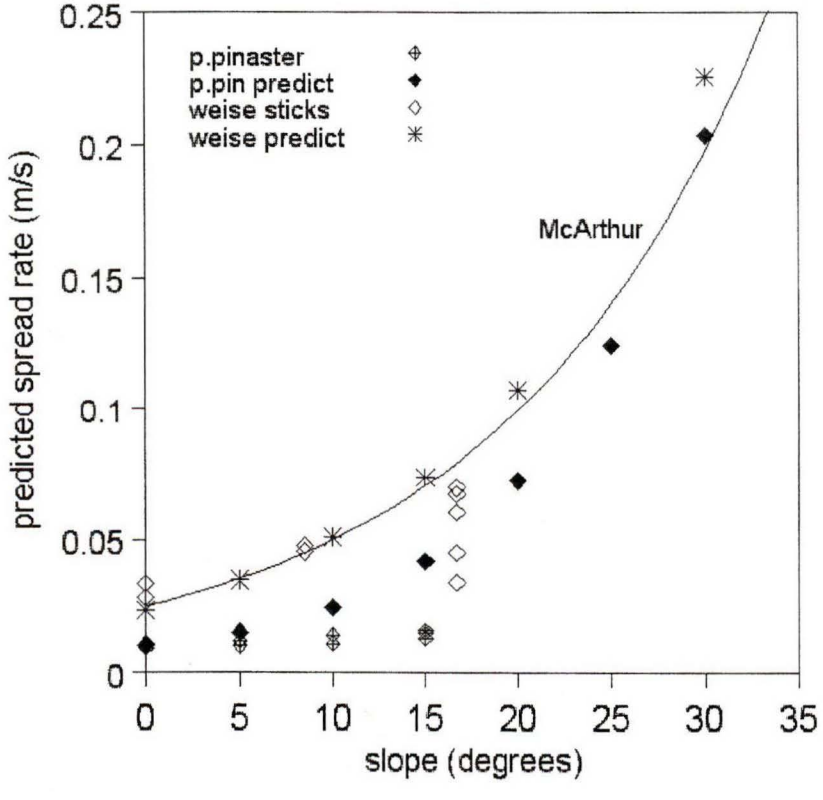

Figure 24. Predicted effect of slope on spread rate in fires in 1m wind, blowing upslope.

Bed width

The flame and combustion zone radiation view factors increase with fuel bed width, but the effect decreases as the bed width increases. Anderson (1969) reports that for zero-wind fires in pine needles the effect of bed width is negligible once the bed is 1m wide. In wind-aided fires Wolff *et al.* (1991) report a linear increase in spread rate with bed width up to 1m wide in a semi-open wind tunnel. Unpublished data belonging to Mike Wotton from Forestry Canada from fires in Ponderosa pine in the open, ignited using a series of different bed widths, are shown in Figure 25. Increase in the radiation view factors was not sufficient to account for the increase in spread rates shown. We hypothesize that as the bed width increases less cool air penetrates round to the front of the fire, and so the heating distance in from of the fire increases. We model this as an increase in λ_d by the factor

$$\Theta_W = 1\text{-}exp(-0.5\ W_0^{0.5}))/(1\text{-}exp(-0.5\ W^{0.5})) \qquad (16)$$

where W_0 is the half-width of the Missoula laboratory bed ($W_0 = 0.5$), and W is the half-width of the fire in question. Predictions are shown in Figure 25. The results are reasonable, but the bed width function may need some adjustment.

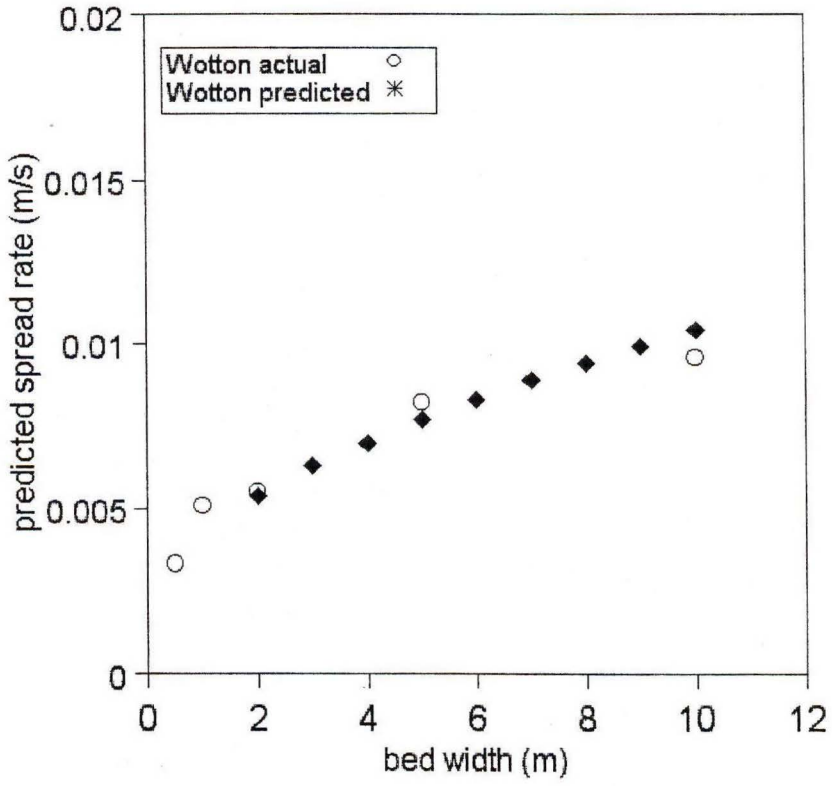

Figure 25. Predicted effect of bed width on spread rate.

Orientation

Although the idea has not been explored, there is potential in the model to take account of fuel orientation by changing the view factor to account for fuel at different orientations. This could be explored using fires in sticks, but the problem of the effect of depth at which the thermocouple is buried in the sticks may make this infeasible.

OTHER CONSIDERATIONS

Mixed fuel

A series of experiments were done with fine fuel (regular and coarse excelsior or pine needles) mixed in among 6mm sticks. Some of these experiments are reported in Catchpole *et al.* (1993). Spread rate was not dependent on the fine fuel used, but was slower than spread rate in fine fuel alone. To model the heat transfer in these mixed fuel fires we consider the heat transfer onto the finest fuel, and use the packing ratio (and loading) of the mixture. For these fuels there is a strong indraft in front of the flame interface caused by the strong buoyancy which reduces the heating distance in from of the fire.

Observed and predicted values for the mixed fuel fires are shown in Figure 16. The model fits the mixed fuel fires as well as the homogeneous fuel fires, but there is some indication that the heating distance in front of the fire is too great at higher wind speeds. Work is needed to modify the heating distance in a way that makes the transition from homogeneous to mixed fuel fires seamless.

Extinction

The model describes fire spread in established fires, and will not predict zero spread rate. Wilson (1985) identified the surface area of fuel per surface area of fuel bed, $s\beta\delta$, and the moisture content as the factors determining whether spread is sustained in zero-wind fires in the laboratory. Marsden-Smedley *et al.* (in press) gave an empirical model for extinction in moorland that depends on wind speed and a factor related to fuel loading or continuity. Live fuel moisture content and the percentage of dead fuel should probably also be factors, as modelled by Rothermel (1972). At this stage it seems easier to follow the example of Wilson (1991) and separate the extinction probability from the spread model, giving a spread rate (however small) together with a probability of extinction. The probability of extinction would need to be developed empirically from ideas in Wilson (1985) and Marsden-Smedley *et al.* (in press), and fitted to available data on conditions where fires failed to sustain. This will be explored in shrubland as part of post-graduate work supported by an ARC grant.

TESTING THE PHYSICAL MODEL ON FIELD DATA

Homogeneous vegetation

Grassland data from Cheney *et al.* (1993) are shown in Figure 26. The grass was cured with some emergent new grass. Average fuel height was 0.35m, average packing ratio was 0.0025, and average moisture content was 5.5%. The treated grass (cut with a harvester) had an average fuel height of 0.14m, packing ratio of 0.006, and moisture content of 6.5%. Predictions from the physical model using the average moisture content and packing ratio are given in Figure 26. The bed width correction in equation (16) was used in the predictions. The model underpredicts spread rate, but not too badly. An adjustment to the surface area to volume ratio (which was set at $3092m^{-1}$) would help, and would reflect the faster spread rate in low packing ratio fires in regular excelsior. The difference in spread rate between natural and treated grass seems quite well modelled. The empirical model badly underpredicts spread rate, and would need a bed-width correction.

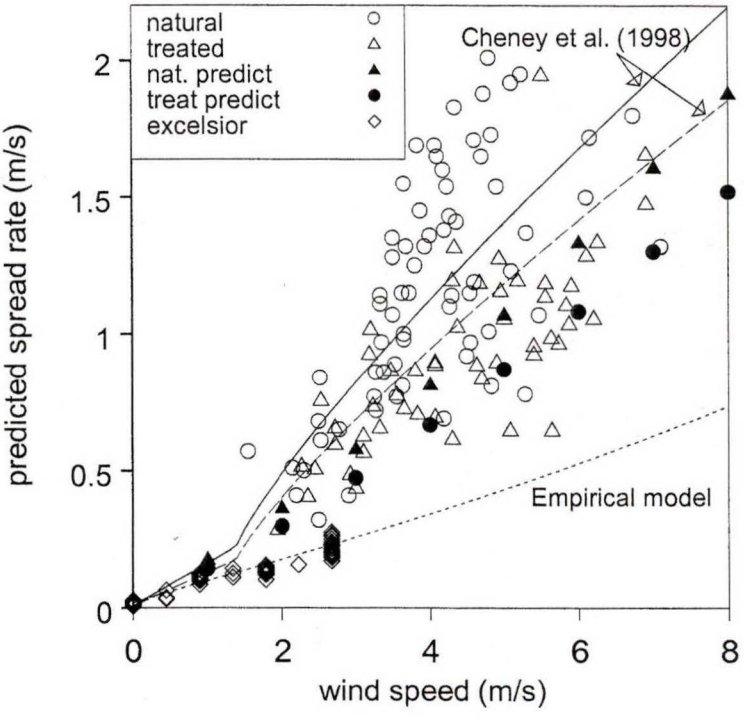

Figure 26. Observed and predicted spread rate in grasslands

The difference in spread rate for grass fires of 50m and 100m, reported by Cheney *et al.* (1993), may be a phenomena that would require a 3-dimensional model of fire spread for explanation. Failing this, it would be necessary to use an empirically-based multiplier such as is presented in Cheney and Gould (1995) to provide predictions for large scale fires.

Field data from fires in forest litter alone (without a shrub component) are rare. It may be found that the shrubs are not significantly affecting spread rate in

many fires, but to be sure we first need to test the model on forest litter. It is hoped that data from fires burned by Marty Alexander (Forestry Canada) will soon be available to test the model.

Live fuel

The data from fires in Tasmanian buttongrass moorland, given in Marsden Smedley and Catchpole (1995) gives us an opportunity to test the model on a fine fuel with a live and dead component. A subset of the data is shown in Figure 27: mature fires of height about 0.3m, packing ratio of about 0.008, dead fuel moisture content about 16 % and the percentage of dead fuel about 40%. To fit the model it was necessary to reduce the flame radiative emissive power by using the overall average moisture content in the fuel complex. The predictions are a bit high, but quite good on the whole.

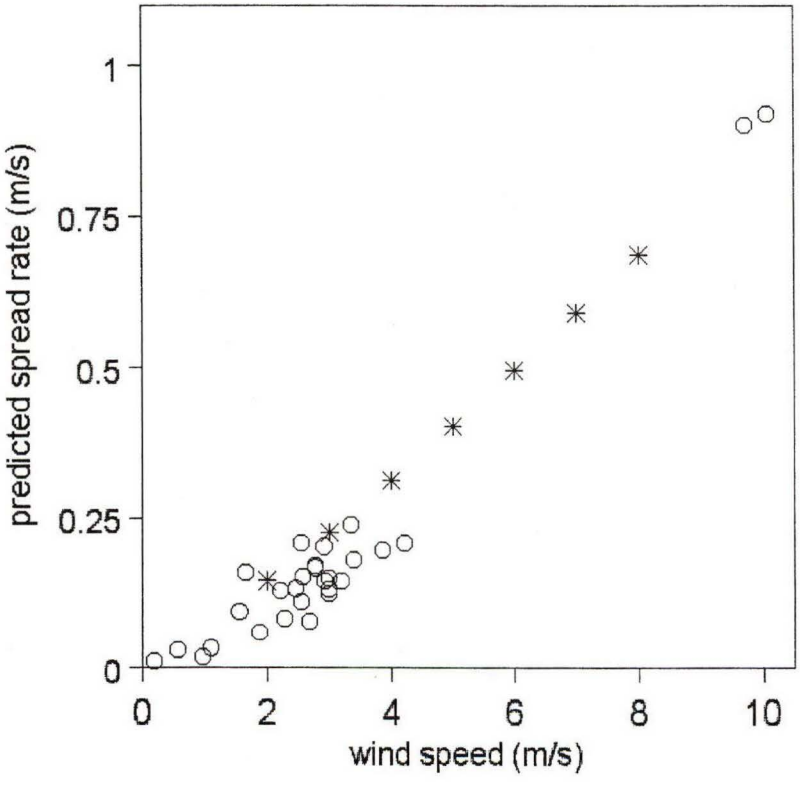

Figure 27. Observed and predicted spread rate in Tasmanian buttongrass moorlands.

SUMMARY

The physical model appears quite viable. It has more flexibility and behaves in a more intuitive manner than the empirical model. The empirical model can be made to fit the available data, but may not behave so well for new data sets. If submodels in terms of physically appealing variables, such as Byram's intensity, can be used without affecting the model's convergence, the behaviour of the model will be more robust.

The physical model has a few disadvantages that can almost certainly be overcome. Firstly it is oversensitive to surface area to volume ratio, particularly at higher packing ratios. This is a major problem, and we may need some adjustment to the real surface area to volume ratio to deal with this. Secondly, convergence is not guaranteed, particularly if the convection term is small. Work is needed on the numerical solution of equation (21) to solve this problem. Thirdly, convergence is slow in Splus (the software package used to develop the program). The last two problems can almost certainly be solved by re-writing the code in C, and using standard library algorithms for the iterative solution of equation (21).

REFERENCES

Albini, F. A. (1981). A model for the wind-blown flame from a line fire. *Combustion and Flame* **43**, 155-117.

Albini, F. A. and Reinhardt, E. D. (1995). Modeling ignition and burning rate of large woody natural fuels. *International Journal of Wildland Fire* **5**, 81-91.

Anderson, H. E. (1969). Heat transfer and fire spread. USDA Forest Service, Intermountain Forest and Range Experimental Station, Ogden, UT, Research Paper INT-69.

Byram, G. M. (1959). Combustion of forest fuels. In 'Forest Fire: Control and Use'. (Ed. K. P. Davis.) pp. 61-80. (McGraw-Hill: New York.)

Catchpole, W. R., Bradstock, R. A., Choate, J., Fogarty, L. G., Gellie, N., McCarthy, G. J., McCaw, W. L., Marsden-Smedley, J. B., and Pearce, G. (1998a). Co-operative development of equations for heathland fire behaviour. Proceedings of 3rd International Conference of Forest Fire Research and 14th Conference of Fire and Forest Meteorology, Luso, Coimbra, Portugal, pp. 631-645.

Catchpole, E. A., Catchpole, W. R. and Rothermel, R. C. (1993). Fire behavior experiments in mixed fuel complexes. *International Journal of Wildland Fire* **3**, 45-57.

Catchpole, W. R., Catchpole, E. A., Rothermel, R. C., Morris, G. A., Butler, B. W. and Latham, D. J. (1998b). Rate of spread of free-burning fires in woody fuels in a wind tunnel. *Combustion Science and Technology* **131**, 1-37.

Catchpole, W. R., Catchpole, E. A., Rothermel, R. C., Morris, G. A., Butler, B. W. and Latham, D. J. Fire behaviour characteristics of free-burning fires in woody fuels in a wind tunnel. (in preparation (a)).

Catchpole, W. R., Catchpole, E. A., Rothermel, R. C., Morris, G. A., Butler, B. W. and Latham, D. J. Flame characteristics of free-burning fires in woody fuels in a wind tunnel. (in preparation (b)).

Cheney, N. P. and Gould, J. S. (1995). Fire growth to a quasi-steady rate of forward spread. *International Journal of Wildland Fire* **5**, 237-247.

Cheney, N. P., Gould, J. S. and Catchpole, W. R. (1993). The influence of fuel, weather and fire shape variables on fire-spread in grasslands. *International Journal of Wildland Fire* **3**, 31-44.

Dupuy, J.L. (1995). Slope and fuel load effects on fire behaviour: laboratory experiments in pine needles fuel beds. *International Journal of Wildland Fire* **3**, 153-164.

Mendes-Lopes, J.M.C., Ventura, J.M.P, Amaral, J.M.P. (1998) Rate of spread and flame characteristics in a bed of pine needles. Proceedings of 3rd International Conference of Forest Fire Research and 14th Conference of Fire and Forest Meteorology, Luso, Coimbra, Portugal, pp. 497-511.

McMahon, C. K., Adkins, C. W. and Rogers, S. L. (1986). A video image analysis system for measuring fire behavior. *Fire Management* **47**, 10-15.

Marsden-Smedley, J. B. and Catchpole, W. R. (1995). Fire behaviour modelling in Tasmanian buttongrass moorlands. II. Fire behaviour. *International Journal of Wildland Fire* **5**, 215-228.

Marsden-Smedley, J. B., Catchpole W.R. and Pyrke, A. Fire behaviour modelling in Tasmanian buttongrass moorlands: sustaining versus non-sustaining fires. *International Journal of Wildland Fire* (in press).

Nelson, R. M. and Adkins, C. W. (1986). Flame characteristics of wind-driven surface fires. *Canadian Journal of Forest Research* **16**, 1293-1300.

Nelson, R. M. (1996). Entrainment and flame characteristics for free-burning fires. Office Report, Fire Behaviour Project – RWU 4401, August 1, 1996.

Pagni, P. J. and Peterson, T. G. (1973). Flame spread through porous fuels. *14th Symposium (International) on Combustion.* pp. 1099-1106. (The Combustion Institute: Pittsburgh, PA.)

Rothermel, R. C. (1972). A mathematical model for predicting fire spread in wildland fuels. USDA Forest Service, Intermountain Forest and Range Experimental Station, Ogden, UT, Research Paper INT-115.

Veigas, D. X. (1999). GESTOSA 98. Shrubland experimental fire general report. Inflame project, ENV4-CT98-0700. Coimbra, Portugal.

Weiss, D. R. and Biging, G. S. (1997). A qualitative comparison of fire spread models incorporating wind and slope effects. *Forest Science*, **43**, 170-180.

Wilson, R. A. (1985). Observations of extinction and marginal burning states in free burning porous fuel beds. *Combustion Science and Technology* **44**, 179-193.

Wilson, R. A. (1990). Reexamination of Rothermel's fire spread equations in no-wind and no-slope conditions. USDA Forest Service, Intermountain Forest and Range Experimental Station, Ogden, UT, Research Paper INT-434.

Wolff, M. F., Carrier, G. F. and Fendell, F. E. (1991). Wind-aided fire-spread across arrays of discrete fuel elements. II Experiment. *Combustion Science and Technology* **75**, 261-289.